universität wien

MASTERARBEIT | MASTER'S THESIS

Titel | Title

Deciphering the Regenerative Potential of Axolotl Limb Connective Tissue Cells

verfasst von | submitted by

Klaus Ehrlinger BSc

angestrebter akademischer Grad | in partial fulfilment of the requirements for the degree of

Master of Science (MSc)

Wien | Vienna, 2025

Studienkennzahl lt. Studienblatt | Degree programme code as it appears on the student record sheet:	UA 066 865
Studienrichtung lt. Studienblatt | Degree programme as it appears on the student record sheet:	Masterstudium Molecular Biology
Betreut von | Supervisor:	Elly Tanaka PhD

Acknowledgments

My sincerest gratitude goes to Elly Tanaka, who has put up with far more than should be necessary for a master student. I once told her that I can not offer anything in return other than my gratitude, to which she replied that this would always be enough. So, thank you very much, Elly!

My direct supervisor, Prayag Murawala, has invested more time into discussing and arguing science and experiments with me, than anyone could ask for. I appreciate this guidance in all the different projects we tackled together.

Christian Aigner from the ProTech facility of the VBCF deserves specific mention, since he was more engaged in supporting me in the production of transgenic baculovirus than he was obligated to.

Siegfried Schloissnig was always available for discussion and moral support around the clock, and gave me the opportunity to work with him on some incredibly ambitious projects after I departed the group, for which I ought to be eternally grateful.

Table of Contents

Abstract

The exact composition of the blastema during regeneration of axolotl limbs is not completely understood. Earlier work showed that paired related homeobox 1 (*Prrx1*) expressing cells play an important role during regeneration, but the extent to which they are involved is unclear. Microarray and single-cell RNA sequencing (scRNA-Seq) experiments shed light on the differential regulation of blastema cells during regeneration, but do not provide sufficient spatial information about the distribution of *Prrx1*$^{+}$ cells in the blastema. In this work we use a combination of Cre-loxP based lineage tracing and fluorescence microscopy to characterize the prevalence of *Prrx1*$^{+}$ cells over time and space in the blastema of axolotl limbs.

Microarray and scRNA-Seq data revealed several genes that show differential expression during limb regeneration, which need to be further investigated. To better understand these genes, scratch assays were carried out to determine the effect of *Prrx1* overexpression on cell motility. Prothymosin-alpha like (*Ptal*), another gene found in microarray and scRNA-Seq experiments, was also functionally characterized by determining the effect of *Ptal* overexpression on cell proliferation.

Knock-out experiments in axolotl are difficult due to several reasons that could be mitigated by employment of in-situ knock-out techniques. Conventional knock-out experiments are usually done by establishing knock-out animal lines. A long generation time of axolotl makes this approach tedious. Another problem is that genes that are implicated in

regeneration likely would lead to embryonic lethality upon knock-out, since regeneration and embryogenesis share a lot of functional genes. In recent years, baculovirus (BV) was proposed as an effective *in-situ* transfection method for axolotl. By local infection of axolotl limb prior to or during regeneration, the desired overexpression or knock-out construct can be introduced without producing transgenic animals. While overexpression of genes with baculovirus was already possible, Cas9 expressing baculovirus has not been successfully produced. By streamlining and optimizing the production protocol, we were able to establish functional Cas9-BV production, which will serve as an important tool for researchers in axolotl.

Zusammenfassung

Die genaue Zusammensetzung des Blastemas während der Regeneration von Axolotl-Gliedmaßen ist nicht vollständig geklärt. Frühere Arbeiten zeigten, dass paired-related homeobox 1 (*Prrx1*) Zellen eine wichtige Rolle spielen, aber es ist unklar, in welchem Ausmaß sie an der Regeneration beteiligt sind. Microarray- und Einzelzell-RNA-Sequenzierungsexperimente (scRNA-Seq) geben Aufschluss über die differentielle Regulation von Blastemazellen während der Regeneration, liefern aber keine ausreichende räumliche Information über die Verteilung von *Prrx1*$^{+}$-Zellen im Blastema. In dieser Arbeit zeigen wir eine Kombination aus Cre-loxP-basierter Zelllinienverfolgung und Fluoreszenzmikroskopie, die verwendet wurde, um die Prävalenz von *Prrx1*$^{+}$-Zellen über Zeit und Raum im Blastema der Axolotl-Gliedmaßen zu charakterisieren.

Microarray- und scRNA-Seq-Daten enthüllten mehrere Gene, die während der Gliedmaßenregeneration eine veränderte Expression zeigen. Um diese Gene besser zu verstehen, wurden Wundheilungsexperimente durchgeführt, um die Auswirkung der *Prrx1*-Überexpression auf die Zellmobilität zu bestimmen. Prothymosin-alpha-like (*Ptal*), ein weiteres Gen, das in Microarray- und scRNA-Seq-Experimenten gefunden wurde, wurde ebenfalls funktionell

charakterisiert, indem die Wirkung der *PTAL*-Überexpression auf die Zellproliferation bestimmt wurde.

Knock-out-Experimente in Axolotl sind aus verschiedenen Gründen schwierig, die durch den Einsatz von in-situ-Knock-out-Techniken gemildert werden könnten. Konventionelle Knock-out-Experimente werden normalerweise durch die Etablierung von Knock-out-Tierlinien durchgeführt. Die lange Generationszeit von Axolotl macht diesen Ansatz langwierig. Ein weiteres Problem ist, dass Gene, die an der Regeneration beteiligt sind, beim Knock-out wahrscheinlich zu embryonaler Letalität führen würden, da Regeneration und Embryogenese viele funktionelle Gene gemeinsam haben. In den letzten Jahren wurde das Baculovirus (BV) als eine effektive *in-situ* Transfektionsmethode für Axolotl vorgeschlagen. Durch lokale Infektion des Axolotl-Gliedmaße vor oder während der Regeneration kann die gewünschte Überexpression oder das Knock-out-Konstrukt eingeführt werden, ohne dass transgene Tiere produziert werden müssen. Durch die Optimierung des Produktionsprotokolls konnten wir eine funktionelle Cas9-BV-Produktion etablieren, die Forschern als wichtiges Werkzeug dienen wird.

Introduction

The current understanding of regenerative biology and its implication for human medical application

Every organism since the development of life on earth faced the possibility of sustaining wounds through outside forces. Especially the life of bigger multicellular organisms is regularly threatened by tissue lesions and physical trauma. While it is not realistic for animals to completely avoid such damage, evolution came up with increasingly complex ways to heal the resulting wounds[123].

Wound healing in vertebrates always follows a predefined pattern: upon a tissue lesion, an event cascade is triggered by signaling molecules, released from damaged cells in the wound and platelets[1]. These signal transmitters are sensed by the surrounding tissue, which enters an inflammatory stage to clear damaged tissue and contamination from the wound site. After approximately 72 hours, this inflammation results in a phase of cell proliferation to close the affected area of damage[3]. Temporal segregation of the inflammatory and the proliferative phase is not very strict, and the onset of cell proliferation usually happens while the inflammatory response to the tissue damage is still active[3]. Most of the damaged tissue is replaced by fibroblasts, which provide a structural scaffold for newly formed tissue by producing the structural protein collagen[4]. Fibroblasts from different lineage origins fulfill distinct roles during wound healing[4]. Recent lineage tracing experiments for example revealed a fibroblast population, originating from the

subcutaneous fascia region, that rise to the wound surface upon injury, carrying with them their extracellular surroundings[5]. This way, they provide a ready-made, provisional wound plug, that contains structural proteins, immune cells and blood vessels[5]. Fibroblasts also facilitate angiogenesis, the formation of new blood vessels in the wound, by secreting matrix metalloproteases (MMP), that clear the extracellular matrix for endothelial cells which form new capillary vessels[4]. In addition to these repair processes, fibroblasts also act as signaling centers, providing molecular cues that stimulate wound healing processes in other cells[4]. After the injury is sufficiently repaired with structural protein, fibroblasts and blood vessels, in a last stage, the produced structures need to be further rearranged to properly carry out their functions[3]. The different mechanisms used during this process, can result in two different outcomes: repair and regeneration[6].

Healing can be grouped in two distinct classes: repair and regeneration

Repair by scar tissue formation is the most common mechanism for wound healing in mammals[1]. Scar tissue is unable to properly carry out the function of the tissue it replaces, but allows surrounding tissue to functionally compensate[1]. Morphologically, scar tissue is composed of the same components as functional tissue. The striking difference between them is the orientation of connective tissue (CT) proteins, most importantly collagen. While collagen is a mesh of basket weaved fibers in healthy tissue, the same collagen fibers are arranged in parallel in scar tissue[1]. As a result of this more homogeneous structure, the resulting

scar tissue is less elastic, making it a suboptimal replacement for the original tissue. Additionally, scars lack functional subunits, such as hair follicles or sweat glands in the skin[1]. While scarring is generally associated with wound healing, it also plays an important role in disease. One of the better-known examples is liver cirrhosis[7]. Prolonged damage to the liver by toxins or viral infections causes progressive replacement of functional liver tissue with scar tissue. This scar tissue lacks the functional subunits of the liver, the hepatic lobules, in the same way scarred skin lacks sweat glands and hair follicles. Therefore, replacement of functional tissue with scar tissue leads to a decrease in liver function.

Unlike mammals, who rely mostly on scarring to repair wounds, more primitive organisms have achieved awe-inspiring feats of healing[8]. These include not only the scar-free healing of wounds after injury, but the ability to faithfully regrow limbs upon amputation[9], or even to reconstitute whole organisms from just a single living cell[10]. This scar-free manner of wound healing is called regeneration[3]. Since it is conceivable that a deeper understanding of regeneration could lead to new medical applications suitable for humans, substantial resources were invested to understand this process in the last few hundred years. Despite this centuries-long attempt to shed light on how animals regenerate scar-free tissue and regrow limbs, only recently has significant progress in understanding of the underlying mechanisms been made. Regeneration is an incredibly complex and heterogeneous process, with different species having evolved distinct mechanisms of regeneration[8].

Different mechanisms for regeneration are found in different organisms

While mammals and other similarly complex animals must resort to imperfect healing mechanisms, simpler life forms can utilize a far more sophisticated toolbox for wound healing.

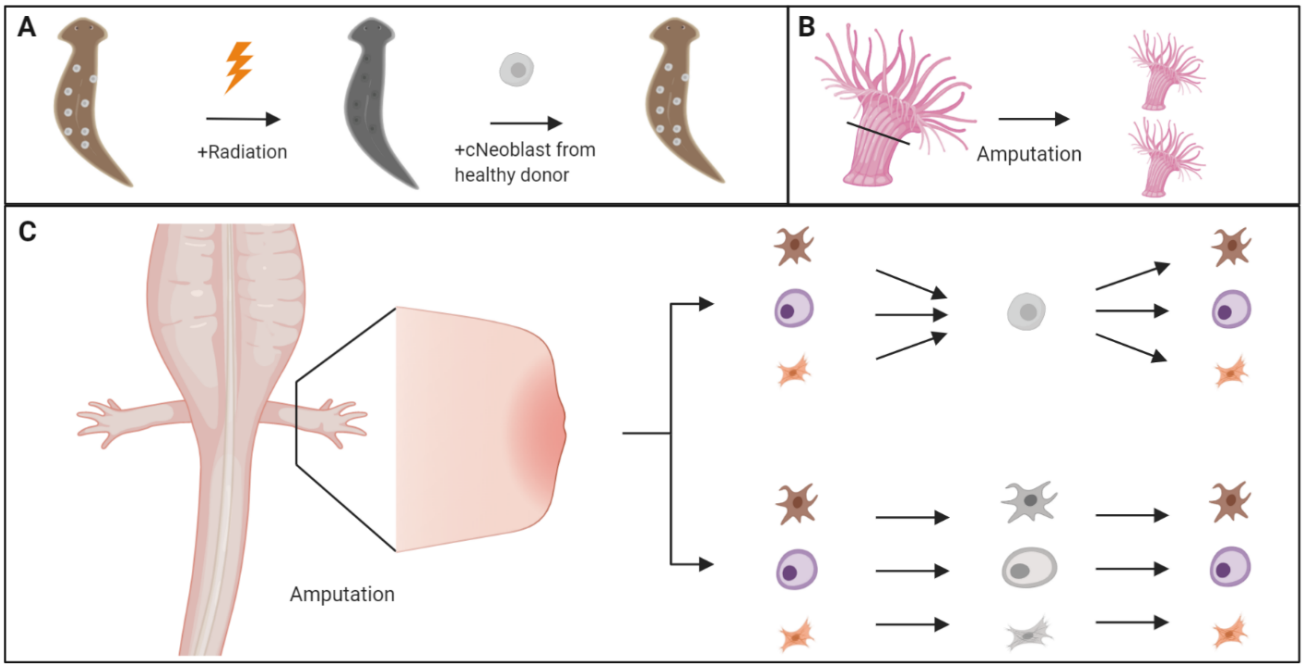

Figure 1: Different regeneration mechanisms A: Stem cell-like regeneration, as found in planaria, relies on pluripotent cell populations called neoblasts. Planaria are irradiated until no more dividing cNeoblasts are present. Upon transplantation of a single cNeoblast from a healthy donor, the irradiated animal completely regenerates from this cell. B: Morphallaxis, a regeneration method in which tissue is restructured without cell proliferation to reconstitute a functional organism. When hydra is cut in two pieces, the separate pieces will undergo reconstruction, and form two smaller sized animals. C: Two different possible dedifferentiation pathways are shown that could explain regeneration in more complex organisms, like axolotl. On top, the dedifferentiation of different cell types towards a common progenitor and subsequent redifferentiation is depicted. Below, different cell types are shown, that dedifferentiate towards lineage restricted progenitor cell types, which then re-differentiate within their respective lineage trajectory.

The most remarkable feats in regeneration are found in simple invertebrates like the planaria, a member of the flatworm phylum. The strategy of planaria to regenerate relies on a dividing somatic cell population, the neoblasts, that act in a similar fashion as stem cells in higher animals[11]. Planaria can regenerate complete animals from small

body parts and even single cells[10]. The type of neoblast that possesses this prodigious regenerative potential is called a clonal neoblast (cNeoblast)[10]. The flatworm's ability to regenerate whole animals from single cells was shown in radiation experiments, where planaria were irradiated to the point where no living neoblast was detectable in the body anymore. Upon transplantation of single, living cNeoblasts into the dead host, it regained the ability to regenerate and was ultimately able to reconstitute the whole animal (Figure 1A)[10]. Planarian cNeoblasts therefore have the intrinsic ability to even regenerate cell types across different germ layers[10]. While stem cell-like cells are a very common avenue to facilitate faithful regeneration, they are far from being the only strategy devised by nature.

Another, otherwise unremarkable, animal that relies, at least partly, on stem cells for regeneration is the freshwater polyp hydra from the phylum of cnidaria[8]. The hydra is made up of two cell layers, the inner endodermal epithelium and the outer ectodermal epithelium. Cells from both epithelia act as continuously proliferating stem cells and replenish their respective cell layers with differentiated epithelial cells[12]. Besides these two distinct cell types, hydra possesses an additional multipotent stem cell population[13]. These interstitial stem cells are located between the two cell layers and responsible for the formation of neurons, secretory cells and gametes[13]. Using these three stem cell-types, hydra can regenerate any lost parts of its body via proliferation of progenitor cells. This mode of regeneration, called epimorphosis, is, in one form or

another, found in most animals. But another outstanding characteristic of hydra is its ability to perform morphallaxis, a special kind of regeneration, wherein the amputated parts of an animal form new animals by reorganization of tissue (Figure 1B)[14], which excludes the need for any kind of proliferation. Hydra has perfected this mechanism to the point where completely dissociated hydra cells can reconstitute a whole animal[15]. Hydra and planaria provide great examples for regeneration in well-studied primitive animals, but until very recently, a detailed understanding of regeneration in vertebrates remained more elusive.

Dedifferentiation was proposed as a mechanism for regeneration in more complex animals. Existing mature tissue in a wound could dedifferentiate into a progenitor state. These undifferentiated progenitor cells could then develop into any cell type needed for the reconstruction of the missing body part. Another, similar approach could be the dedifferentiation of different cell types from the wounded body part into lineage restricted progenitor cells, these would subsequently regenerate missing cell types within their respective cell lineage (Figure 1C). Both these explanations were equally plausible for a very long time, since molecular and cellular biological tools for the investigation of these two scenarios were lacking[8]. Recently, the advent of new lineage tracing methods has significantly furthered our understanding of these processes during regeneration, as shown below.

These three examples illustrate the diversity of regeneration found in nature. To translate the understanding of regeneration in model

organisms to medical applications in humans, it is necessary to study all aspects of regeneration found in a broad range of different species. With respect to the endeavor to enhance human healing capacities, it is necessary to consider how likely different regeneration approaches could translate into humans. It is for example imaginable that morphallaxis in hydra is only possible because the body plan that needs to be reconstituted is sufficiently simple. Reconstituting a complex structure like the human body from just a severed hand seems highly implausible, even with sophisticated genetic engineering employed to achieve this goal. The reliance of animals like flatworms on distinct stem cell-populations for regeneration, on the other hand, was already an inspiration to use cells with such enhanced potency for therapeutic applications[16]. Although tremendous advances in the field of stem cell-therapy occurred, there is still a long way until reconstitution of complex structures is possible by these means.

Humans possess a limited inherent regenerative potential

While scarring is the most prominent healing process in mammals, even complex animals like humans have limited regenerative potential[3,17,18]. For centuries, doctors have documented medical cases that illustrate regeneration in humans. The most noteworthy example is the ability of mammalian fetuses to regenerate skin without the formation of scars in the first two trimesters[17]. Despite decades-long efforts to determine the cause for this enhanced regenerative potential, the exact differences between embryonic and postnatal healing remain poorly

understood (for review see Wilgus, 2006). Limb regeneration in salamander seems to recapitulate certain stages of the embryonic limb-bud development[19]. The implication being, that the genetic program needed for regeneration is probably still present in adult mammals but is shut off after a certain point in development. The fact that regeneration is widespread in primitive organisms and was evolutionarily lost in complex animals, is reconcilable with the mirrored loss of regeneration during mammalian development. Identifying the causes for the loss of regenerative potential during development and reconstituting elements needed for regeneration in adults should be a major goal of further research.

In parallel to developing embryos, humans still possess a limited capacity for scarless healing and regeneration until well into adulthood. Skin wounds with a thickness of less than two millimeter heal without scarring[18]. This led in 2016 to the development of a technique able to reconstitute skin tissue in macroscopic wounds by transplanting microcolumns of skin from uninjured body regions. Clever use of readily available tissue regeneration in humans should be considered for potential therapeutic applications in the future, since they do not require any form of genetic engineering or external tissue supplementation.

In the future, many roads could lead towards augmented regenerative potential in humans. Some seem easier to achieve than others. Scar free healing of minor skin lacerations or reduction of scarring in organs following disease could potentially be achieved by using drugs or

exploiting naturally occurring healing mechanisms in clever ways. The regeneration of severed limbs on the other hand will probably demand more involved, possibly genetic, alterations to the patient. Investigating how the human body manages wounding is certainly necessary, but to truly revolutionize wound treatment, studies of regenerating model organisms are needed. The understanding of, for example, morphallaxis in hydra is an important step towards gaining a more complete picture of how regeneration evolved, but it will probably be unimaginably difficult to translate this knowledge directly to humans. It would be wise to look at our closer phylogenetic neighborhood for another organism that is endowed with immense regenerative potential. One that is closely enough related to us that our morphologies are at least superficially similar.

The axolotl is a prime example for a model organism in regenerative biology

The axolotl is a salamander species that can not only repair damage to the spine, various organs and even the brain, but can also regrow lost appendages like limbs and tails[9]. The axolotl brings another advantage to the table, which more primitive organisms like planaria and hydra lack: the salamander is a tetrapod, meaning its body plan includes four appendages, making them very similar to humans. The close phylogenetic relation between humans and axolotl makes it likely that understanding of axolotl regeneration can be more directly applied to mammals.

The current understanding of the regeneration process in axolotl suggests that there are two main stages: upon amputation of a limb, the epidermal cells around the amputation plane migrate to cover the wound (Figure 2A)[8]. The exact role of the resulting wound epidermis is still not completely understood, but recent data suggests that it acts as a source of signaling molecules that induce downstream processes like migration of CT cells towards the amputation site and cell proliferation to replenish the lost tissue mass[20]. In the next step, cells in the source zone - a region of 50-500µm adjacent to the amputation plane - form a structure of undifferentiated mesenchymal cells, the blastema[21]. This cell mass is responsible for the subsequent reconstitution of the lost limb by inducing migration, proliferation, differentiation and patterning of cells into tissue of the lost appendage. A crucial step during this regeneration process is the coalescence of CT cells towards a multipotent progenitor state. How this concerted dedifferentiation effort progresses, was recently elucidated using a combination of Cre-loxP-based lineage tracing (Figure 2B) and single cell scRNA-Seq[19]. Knapp, Murawala and Gerber showed how heterogeneous CT cell populations from the blastema transition towards a common, limb bud-like progenitor state, and resolved the lineage progression of distinct cell types towards regenerated tissue. In accordance with older data[2223], they saw that blastema cells retain a memory of their tissue origin and were only able to regenerate tissue within their respective lineage restrictions. Examination of the cellular dynamics underlying limb regeneration is important to identify the

genetic protagonists involved in this process, but to properly dissect the regulatory network behind limb regeneration, functional analysis of these genes is required.

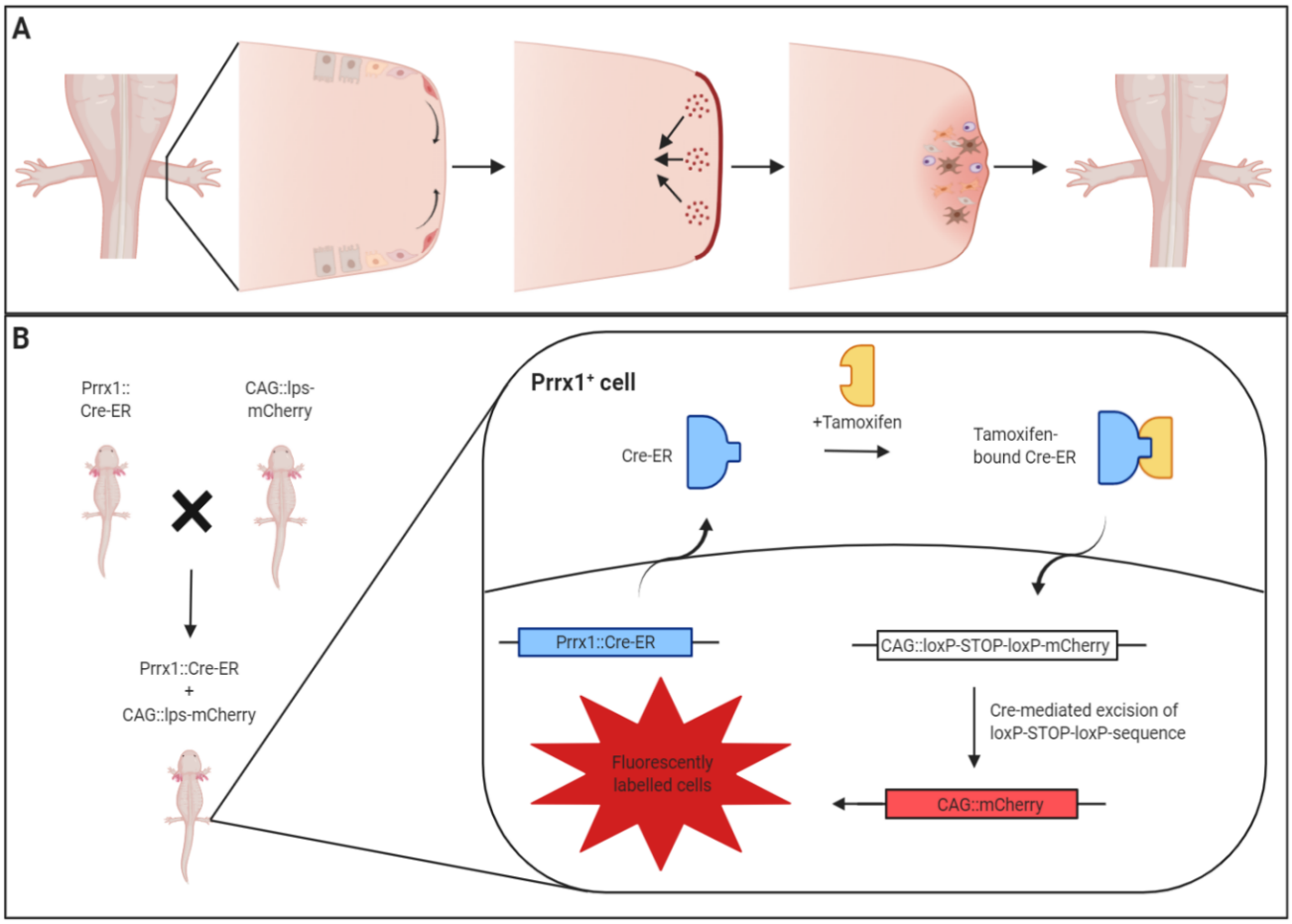

Figure 2: A: Event cascade triggered in axolotl upon limb amputation. In the first 24 hours after amputation, the amputation plane is covered with wound epithelium (shown in red, middle). The wound epithelium acts as a signaling source for cells adjacent to the amputation plane, which then start to form the blastema, a mass of undifferentiated cells that reconstitutes the missing limb. B: Schematic of Cre-loxP based lineage tracing method. Two transgenic animals are crossed. One contains a tamoxifen inducible Cre gene (Cre-ER) under control of the Prrx1 promoter, the other contains the strong, constitutive CAGGS promoter, followed by a loxP-flanked stop-sequence and the mCherry reporter gene. The result is a Prrx1::Cre-ER / CAGGS::loxP-STOP-loxP-mCherry animal. Upon tamoxifen administration, the stop-sequence in front of the mCherry gene is removed by Cre, and Prrx1+ cells and their descendants are marked with stable mCherry expression.

To design robust functional assays, for example Cas9-mediated loss of function screens, the genomic sequence of the axolotl is needed. The assembly of the axolotl genome was difficult, due to its gargantuan size

of 32 gigabases - which is roughly 10x the size of the human genome - and the presence of long intronic repeat sequences. Such repeats are not resolvable with conventional short-read next-generation sequencing techniques. In breakthrough-work published in 2018, Schloissnig, Nowoshilow et al were able to assemble the axolotl genome at unprecedented fidelity, using a novel assembler called MARVEL. This tool relies on a combination of long-read sequences to achieve large-scale contiguity, and short-read sequences for sequence correction on a base pair level[24]. The analysis of the genomic data from axolotl already gave important insights into the evolutionary development of the genome and allowed identification of regeneration-associated genes with orthology limited to closely related vertebrates. In the future, research on chromosome dynamics in axolotl via methods like HiC will be possible using this genomic data, techniques like ChIP-Seq can now be used to investigate protein-DNA interactions, and as mentioned earlier, Cas9-based functional screens will be an important area of work when moving forward. CRISPR-Cas9 approaches rely on the identification of appropriate guide RNA target sequences in the genome, which was made possible by the recently acquired genome data. The sequencing and assembly of the axolotl genome was a critically needed milestone for axolotl research and will open new avenues to understand regeneration in this animal.

Loss of function screens in axolotl are problematic, because the axolotl has a very long generation time of roughly one year, making the creation of transgenic lines time consuming[25]. Additionally, genes involved in

regeneration often play a role during development, meaning knock-out of these genes can result in embryonic lethality[26]. These problems could be circumvented, by doing *in-situ* somatic knock-out experiments in the adult animal. Reliable methods for genetic manipulation of adult animals are still lacking, making the adaption of such a vector system a high priority. Baculovirus (BV) is an insect cell-derived vector, initially established as a protein expression system, but recently adapted to transfect vertebrate cells[27]. The biggest advantage of the system is its ability to insert huge DNA fragments into the target[27]. Cas9-based assays often rely on DNA fragments upwards of 10kb in size[26], which is near the limit of what conventional methods can transfect[28]. The field of genome editing has seen a surge in new methods combining Cas9 with various other enzymes to increase specificity and efficiency[29]. As these tools get more sophisticated and rely increasingly on simultaneous transfection of numerous large proteins into the target cell, a vector system that does not restrict its user in insert size becomes more and more valuable. Establishing baculovirus as a gene-delivery tool would be a convenient way to circumvent a long generation time, potential embryonic lethality of gene knockouts, and fragment size-restriction during transfection in axolotl and other organisms.

The goal of this thesis was to develop methods to functionally study how *Prrx1*-expressing cells in the adult limb form the regeneration blastema. Towards that aim, I characterized the kinetics by which *Prrx1*$^{+}$ cells accumulate in the blastema. I used two in-vitro assays coupled with

baculovirus-mediated over-expression to study two candidate regulators of *Prrx1*$^{+}$ cells. Finally, I attempted to establish Cas9 expressing baculovirus as a somatic knock-out system.

Results

Connective tissue cells are the main contributors to blastema formation

At the center of limb regeneration is the blastema, a structure of undifferentiated cells that is responsible for the reconstitution of the functional limb[8]. Despite significant progress in the last decades, a thorough understanding of the mechanisms involved is still lacking. PRRX1 is a transcription factor that is upregulated in cells of the mesodermal limb bud[30]. These cells later form mesenchymal limb CT cells, which retain *Prrx1* expression[31]. Blastema formation relies heavily on these *Prrx1*$^{+}$ CT cells, and they have been the focus of a lot of research in the past. The specific contribution of CT cells to the regenerating appendage was, for example, investigated by tracking CT cell movement during regeneration[21]. Hereby, Currie et al could show that different subpopulations of CT cells are reconstituting different appendage segments during regeneration. Further work characterized the dynamic development of *Prrx1*$^{+}$ CT cells over the course of regeneration using scRNA-seq [19]. This approach revealed the existence of a transitional, limb bud-like state, adult CT cells pass through, before reconstituting the regenerated limb. While providing significant insight into the role and behavior of CT cells during regeneration these experiments did not

provide a quantitative assessment of how many blastema cells are descendants of *Prrx1* expressing CT cells. The following experiment, based on Cre-loxP mediated lineage tracing, coupled with microscopic analysis, set out to answer this question, and investigate the spatiotemporal distribution of *Prrx1*-expressing cells during axolotl limb regeneration.

Quantitative analysis of spatiotemporal *Prrx1*$^+$ cell distribution in the blastema

Prrx1$^+$ cells in both the blastema and source zone were identified by *mCherry* expression and antibody staining of PRRX1. To trace *Prrx1*$^+$ cell distribution throughout the blastema, a transgenic *Prrx1*::Cre-ER/CAGGS:lp-*mCherry* axolotl line was used[19]. In these animals, a tamoxifen inducible version of the Cre recombinase is expressed under control of the *Prrx1* enhancer element. Upon tamoxifen administration, the recombinase is transported into the nucleus, where it removes a loxP flanked stop sequence from the CAGGS:lp-*mCherry* construct, which leads to the stable expression of *mCherry* in *Prrx1*$^+$ cells. After subsequent amputation of forelimbs, longitudinal sections of the regenerating blastema were made at different timepoints after amputation. The timepoints were chosen based on significant changes in expression profiles of blastema cells[22], as well as the cell cycle length of blastema cells[32]. Sections were analyzed from the uninjured and freshly amputated limb, as well as blastema from 3, 5, 7, 10, and 14 days post amputation (dpa). These sections were stained with anti-PRRX1 antibodies, and analyzed using a slide scanner, a microscope that allows the automated,

spatially comprehensive inspection of large samples. The combination of genomic *mCherry* expression and antibody staining was necessary, since previous experiments have shown that Cre/ loxP conversion only leads to *mCherry* expression in 80% of all *Prrx1* expressing cells[19]. The double staining approach, along with strategically chosen timepoints to analyze the blastema, resulted in a sufficiently strong dataset to draw conclusions about the quantitative development of *Prrx1* -expressing cells in the blastema.

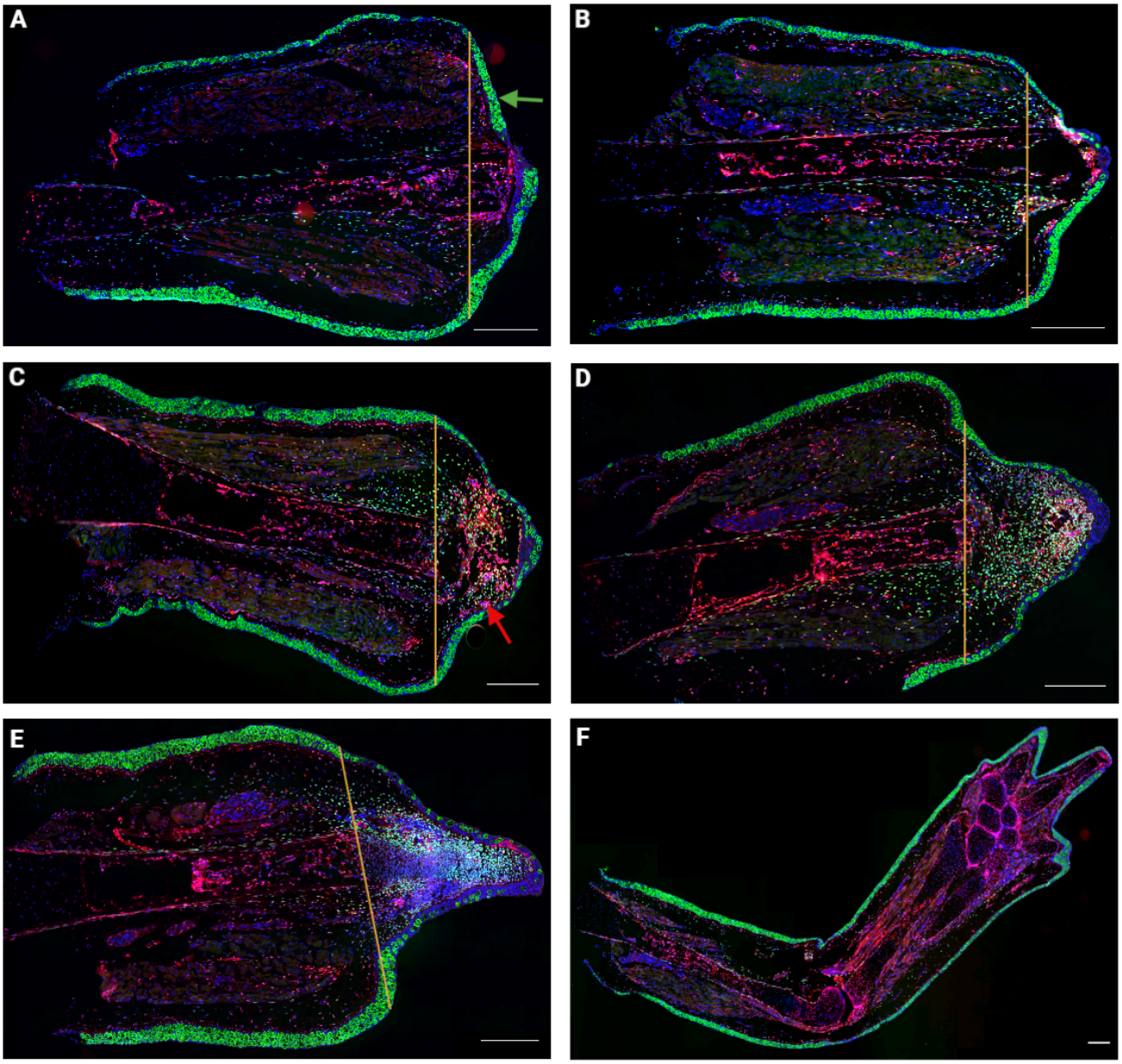

Figure 3: A-F: Sections of the axolotl forelimb at 3, 5, 7, 10, and 14 days post amputation (dpa) and mature unamputated for reference. Not shown are sections from the freshly amputated limb. Prrx1+ cells are marked by mCherry expression, shown in red, and antibody staining, shown in green. Counterstaining was done using DAPI, shown in blue. The amputation plane is shown in orange. Green structures on the edge of the sections are epidermal cells (green arrow in A). Clearly visible in C are clusters of red blood cells in the blastema (red arrow), distinguishable from Prrx1+ cells by a distinct absence of signal in their center. Neither blood cells, nor epidermal cells were counted in this experiment. E: At 14 dpa, the Prrx1- cells start clustering at the proximal part of the blastema in a roughly arrow-shaped pattern. F: Section of the mature, unamputated forelimb.

The different cell types were classified into three categories: *Prrx1*$^{+}$ cells, *Prrx1*$^{-}$ cells, and bone cells (Table 1). Classification was done in both the regenerating blastema, as well as the adjacent source zone of 500 µm

proximal of the amputation plane. From each timepoint, five sections were taken from three animals, respectively. Due to imperfect sectioning or problems during microscopy, we were not able to quantify every section separately. We therefore decided to only analyze the three sections per animal that gave the most satisfying microscopy images (examples shown in Figure 3), generating nine analyzed sections each, for seven timepoints, resulting in 45 analyzed sections. The sum of *Prrx1*$^{-}$ and Prrx1^{+} cells for each timepoint in the blastema and the source zone, respectively, was analyzed.

Table 1: Classification of different cell types in sections of the axolotl limb and their contribution to blastema formation.

Category	Phenotype	Cell type	Note
Prrx1^{+}	DAPI + mCherry DAPI + PRRX1 DAPI + mCherry + PRRX1	Periskeletal cells Dermal CT cells	Main contributors to blastema formation
Prrx1^{-}	DAPI	Muscle cells Nerve cells	No significant contribution to blastema formation
Bone cells	DAPI + mCherry DAPI + PRRX1 DAPI + mCherry + PRRX1	Skeletal cells	*Prrx1*$^{+}$ phenotype, but no significant contribution to blastema formation

An increase in the proportion of *Prrx1*$^{+}$ cells in the blastema, to over 90% demonstrates their importance during blastema formation. The number of *Prrx1*$^{+}$ cells in the blastema went above 2500 over the course of the experiment (Fig 4A). While this increase in *Prrx1*$^{+}$ cells could be explained by general proliferation following limb amputation, we also saw the percentage of *Prrx1*$^{+}$ cells in the blastema reach around 90% at 14 dpa (Figure 4B), showing that this cell population is the main contributor to the formation of the blastema. In contrast, the number of *Prrx1*$^{+}$ cells in

the source zone never exceeded 500 (approximately 55% of all cells in the source zone, Figure 4). The distribution of *Prrx1*$^{+}$ cells in the blastema is relatively uniform until 10 dpa. Starting from 14 dpa, an arrow-shaped cluster of *Prrx1*$^{-}$ cells forms at the proximal end, with few single *Prrx1*$^{-}$ cells dispersed at the distal end of the blastema (Figure 3E). Using this microscopy focused approach in combination with novel lineage tracing methods, we were able to show a steep increase in the proportion of Prrx1^{+} blastema cells after 3 dpa, reaching a maximum of up to 90% two weeks after amputation.

Having characterized the *Prrx1*$^{+}$ cells *in-vivo*, the next goal was to study molecules that affect cell function, first by establishing the baculovirus expression system, and then using it for functional studies.

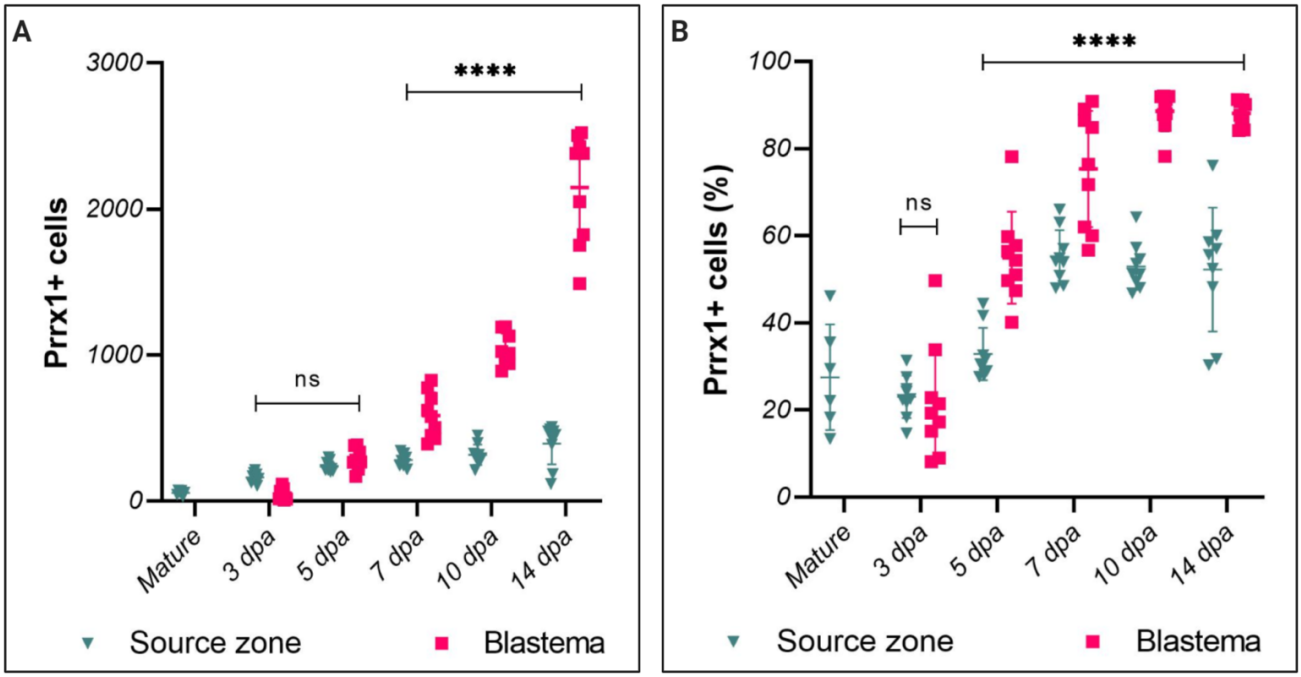

Figure 4: A: The total number of Prrx1^{+} *cells in the source zone and blastema of the respective tissue sections. B: The percentage of Prrx1+ cells in the source zone and blastema. (Multiple t-tests, Two-stage linear step-up procedure of Benjamini, Krieger and Yekutieli, Q = 1%. Computations assume that all rows are sample from populations with the same scatter (SD), ****=p<0,0001, ns= non-significant).*

Baculovirus production was relocated to Vienna and production protocol was optimized

Baculovirus (BV) is of great interest as an *in-vivo* gene transfection vehicle, especially Cas9 expressing BV. Baculovirus is a commonly used system for protein overexpression. The insect cell cultures used to propagate BV can not only synthesize large amounts of protein, but also apply various post-translational modifications to the desired products. The popularity of baculovirus in the protein synthesis field makes it easy to establish production in any facility offering such services. The production protocol is explained in detail in the methods section of this thesis. In summary, the procedure is based on co-transfection of a bacmid, containing a replication incompetent viral genome, and a shuttle vector, providing the recombinant cassette of interest as well as two genes missing for reproduction, into SF9 cells (Figure 5). The two defective genes are *Lef2* and *Orf1650*, both of which contain partial deletions in their respective c-terminal end. The co-transfected shuttle vector provides these missing gene sequences and allows for reconstitution of a replication competent viral genome via homology directed repair. The virus is subsequently propagated by consecutive rounds of infection of increasingly large volumes of insect cell culture. The resulting viral culture is then concentrated and purified via ultracentrifugation steps in sucrose gradients. After this procedure, the produced virus is titrated by dilution series on SF9ET cells, an insect cell line that expresses GFP under control of a viral promoter, leading to a

fluorophore signal in presence of BV. While this protocol was reliably used to produce most BV, synthesis of the highly sought-after Cas9-expressing BV (Cas9-BV) repeatedly failed. Our goal was therefore to optimize the production protocol towards successful Cas9-BV production.

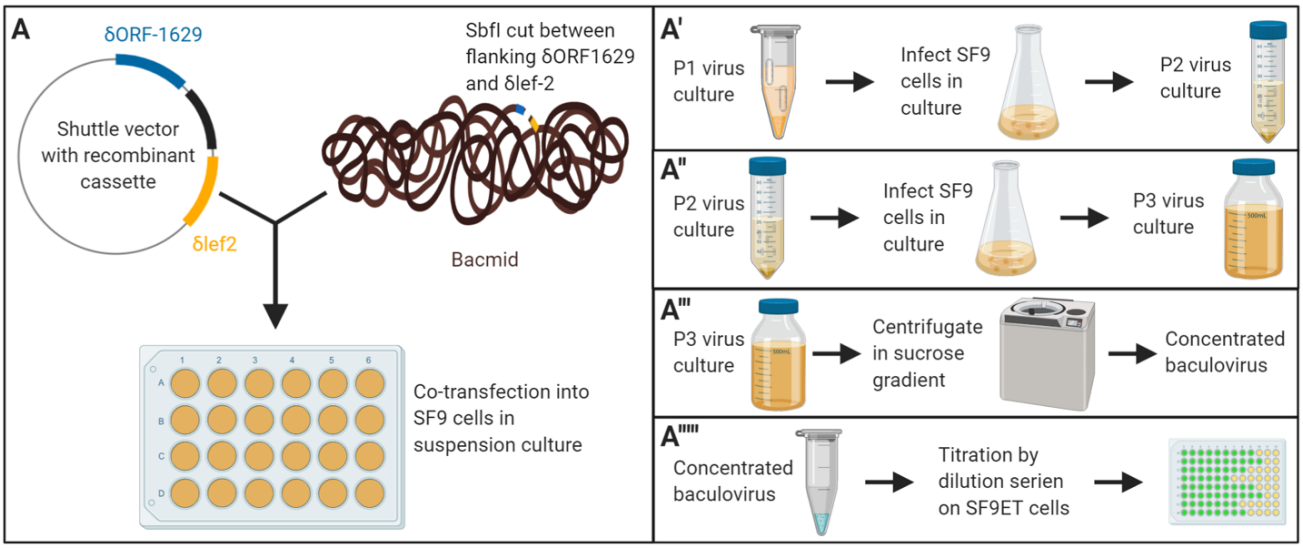

Figure 5: A: Co-Transfection of a bacmid containing a replication incompetent baculovirus (BV) genome and a shuttle vector, containing the desired recombinant cassette and repair templates for the defective genes in the viral genome on the bacmid, into SF9 cells. A': The resulting viral suspension is called P1 and propagated by infection of increasing volumes of SF9 cultures (A"). A"': The final viral suspension, resulting from a 500mL SF9 culture, is concentrated by sucrose gradient centrifugation. A"": The concentrated virus is titrated by dilution series on SF9ET cells. These express GFP under control of a viral promoter and allow visual detection of viral infection.

Examination of the existing Cas9-BV production pipeline and its faulty products revealed potential causes for the failed virus formation. We observed several irregularities during Cas9-BV preparation, summarized in Table 2. At various quality checkpoints during production, we observed signs for successful formation of BV. Bloating of SF9 cells after P1 transfection is one of the hallmarks for successful BV infection, and even more strikingly, when performing a dilution series titration on SF9ET cells, we observed GFP expression, which is an even clearer indicator for the

presence of BV. These findings are contradicted by the absence of fluorophore marker expression in SF9 cells after transfection, and ultimately failure of the concentrated Cas9-BV sample to induce gene expression in AL1 cells. We decided to focus on optimizing the initial P1 transfection step to solve these problems. Missing fluorophore expression after P1 transfection made it very likely that the Cas9-BV production failed at this first step, and measures to improve efficiency were easily implemented.

Table 2: Irregular observations during Cas9 expressing baculovirus (Cas9-BV) production. Bold: Observations differing from expectations.

Stage	Expectation	Observation	Interpretation
Baculovirus (BV) propagation	SF9 cells bloated	SF9 cells bloated	SF9 cells infected with BV
BV propagation	Fluorophore$^+$ SF9	**Fluorophore$^-$ SF9**	SF9 cells not infected with BV
Titration on SF9ET	GFP$^+$ SF9ET	GFP$^+$ SF9ET	BV present
AL1 infection	Fluorophore$^+$ AL1	**Fluorophore$^-$ AL1**	BV defective

Purity and structural integrity of the bacmid, as well as stoichiometry of bacmid and shuttle vector were optimized, and the effect of these changes experimentally determined. To efficiently induce homology directed repair in SF9 cells of the defective genes on the bacmid, the bacmid is cut exactly between these two gene fragments using the SbfI restriction enzyme. The enormous size of the bacmid makes the resulting loose ends prone to shear forces. Preparing fresh bacmid digests for each transfection should decrease the physical stress on these double strand breaks and increase the recombination efficiency between shuttle vector and bacmid. Another factor that could play a role during the initial transfection process is the ratio of bacmid to shuttle vector in the

transfection. The massive difference in size leads to an imbalance of shuttle vector to bacmid particles in favor of the smaller shuttle vector. Increasing the amount of bacmid in the transfection could balance this asymmetry. In addition to increasing the amount of bacmid, we also experimented with simultaneously increasing the amount of shuttle vector and bacmid, to investigate the effect of an overall higher amount of DNA in the reaction, as well as decreasing the amount of shuttle vector at the highest bacmid levels, to establish an extreme disproportion towards bacmid input. This experiment was performed with shuttle vector constructs that were successfully used for BV production, and the results are shown in Table 3. No significant change in fluorophore expression can be detected among different bacmid to shuttle vector ratios and DNA amounts, which leaves bacmid purity as the last avenue to potentially improve recombination efficiency at the first stage of BV production. Since this was done after I left the lab, these results are not shown here, but the implementation and effect of it is discussed below. In summary, structural integrity of the bacmid at the time of transfection was optimized, and the effect of variations in input-stoichiometry were experimentally determined but showed no significant influence on the recombination efficiency in SF9 cells. Cas9-BV production was eventually established by increasing bacmid purity before transfection in SF9 cells.

Table 3: Percentage of Fluorophore+ cells at different levels of bacmid and shuttle vector input (n=1).

Bacmid (ug)	**Shuttle vector (ug)** [ns]	**Bacmid:shuttle vector ratio** [ns]	**DNA amount (ug)** [ns]	**Fluorophore$^+$ cells (%)**
1	1	1:1	2	2.6
4	1	4:1	5	3.2
6	1	6:1	7	3.4

8	1	8:1	9	2.8
8	2	4:1	10	2
10	0.5	20:1	10.5	3.5

Note. Correlation of percentage of Fluorophore$^+$ cells with amount of bacmid, amount of shuttle vector, absolute amount of DNA and bacmid:shuttle vector ratio, respectively, was calculated using the Pearson correlation coefficient with a two-tailed P-value. Confidence interval is 95%.

Functional analysis of genes implicated in regeneration

After streamlining the BV production, we wanted to shed light on the function of two genes that are differentially expressed during regeneration in axolotl limb CT cells. Besides the *Prrx1* gene, we also wanted to determine the function of another gene, Prothymosin alpha-like (*Ptal*). *Ptal* showed interesting expression patterns in scRNA-Seq and microarray data and has no known orthologues in non-regenerating species[19,22]. The following section explains how we set out to characterize the roles of these regeneration-associated genes, using BV for gene transfection.

Effect of *Prrx1*$^+$ overexpression on AL1 cell motility

An implication of Prrx1 in cancer metastasis hints at a potential function of the gene as a regulator of cell motility during limb regeneration. During metastasis, two cellular processes known from development play an important role[33]. Epithelial-to-mesenchymal transition (EMT) describes the change of an epithelial cell, into a more mobile, mesenchymal state. Mesenchymal-to-epithelial transition is the inverse process, allowing cells to attach to tissues and remain fixed in place. Epithelial-to-mesenchymal-plasticity (EMP) is important during metastasis, because it allows the dissociation of cells from a tumor, and

reattachment to other tissues[34]. In cancer biology, PRRX1 is a suspected inducer of EMT[35]. Additionally, the transition between mesenchymal and epithelial identity also plays a crucial role in development. Gastrulation and neural crest formation are two processes that rely heavily on cell migration. Recently, a gene-regulatory network was identified that controls EMP by expression of the transcription factors zinc-finger protein SNAI1 and PRRX1. Based on this knowledge, we speculated that *Prrx1* upregulation during regeneration could confer the cell motility necessary to organize limb structures during regeneration.

Since *in-vivo* experiments to determine gene function are very time-consuming, we decided to use an *in-vitro* approach that allowed for a higher throughput of experiments. The wound-heal- or scratch-assay is a commonly used technique to determine cell motility during wound healing[36]. In this assay, a cell culture is grown to confluence. Upon reaching a confluent monolayer, the cells are scratched with a pipette tip to simulate a wound *in-vitro*. The cells will then try to close the introduced scratch by migration, which is captured by microscopy images over the course of a day. The time needed for the cells to close the scratch is used as a measurement for cell motility. Typically, a wild-type (wt) cell line is used as a control group, along with several transfected test groups. We were using the AL1 cell line for our approach, a cell line derived from axolotl limb CT cells, which we transfected with BV.

We investigated the effect of *Prrx1* overexpression on wound healing behavior of AL1 cells in different culture conditions. Cells were infected

with CAGGS:: *Prrx1*-mCherry virus to determine the effect of *Prrx1* overexpression on cell motility. Specifically, we wanted to know whether *Prrx1* overexpression leads to a change in wound healing speed. *mCherry* mock-virus was used as a negative control, to see how cells behave in presence of BV, without the effect of *Prrx1* overexpression. To control for any adverse effects of general virus infection on cells, uninfected samples were also included in the experiment. Each of these three groups was subjected to four different growth conditions to investigate the effect of *Prrx1* overexpression on AL1 cells in different culture environments. In the first condition, cells were grown in regular high-serum minimum essential medium eagle alpha modification (AMEM), containing 10% fetal calf serum. In this condition, we were expecting the highest healing rate, and it therefore served as a baseline for wound healing speed. A second test condition, where the cells were grown in continued serum starvation (0.1% fetal calf serum), was used to see how cells would behave in the absence of bovine serum proteins. Serum starvation conditions are known to greatly interfere with cellular fitness, since the cells rely on serum proteins to function properly in culture[37]. In a third condition, we cultivated cells that were exposed to a 24-hour serum starvation-pulse prior to injury but could heal in high serum medium to mitigate the negative effects of serum starvation. The latter two conditions were used to identify a suboptimal healing speed. The last experimental condition was a 24-hour serum starvation-pulse in a platelet derived growth factor BB (PDGF-BB) supplemented medium. PDGF-BB was implicated in

blastema cell chemotaxis in earlier work[21]. By incorporating PDGF-BB into this assay, we wanted to see if we could reproduce these results with AL1 cells, and whether PDGF-BB addition was sufficient to mitigate any adverse effect of the serum starvation-pulse on AL1 cell motility. The combination of different overexpression and culture conditions resulted in 12 different experimental groups. The confluent, baculovirus-infected cultures were imaged for 24 hours in 10-minute intervals from the introduction of the scratch until closure of the wound (Figure 6 A and B). The time needed for wound closure, and the approximate number of fluorophore-expressing cells was determined for every observed location, and the results are shown in Figure 6 C and D, respectively. The goal of this experiment was to find out whether *Prrx1* overexpression would influence the healing speed and could make up for the stress of serum starvation.

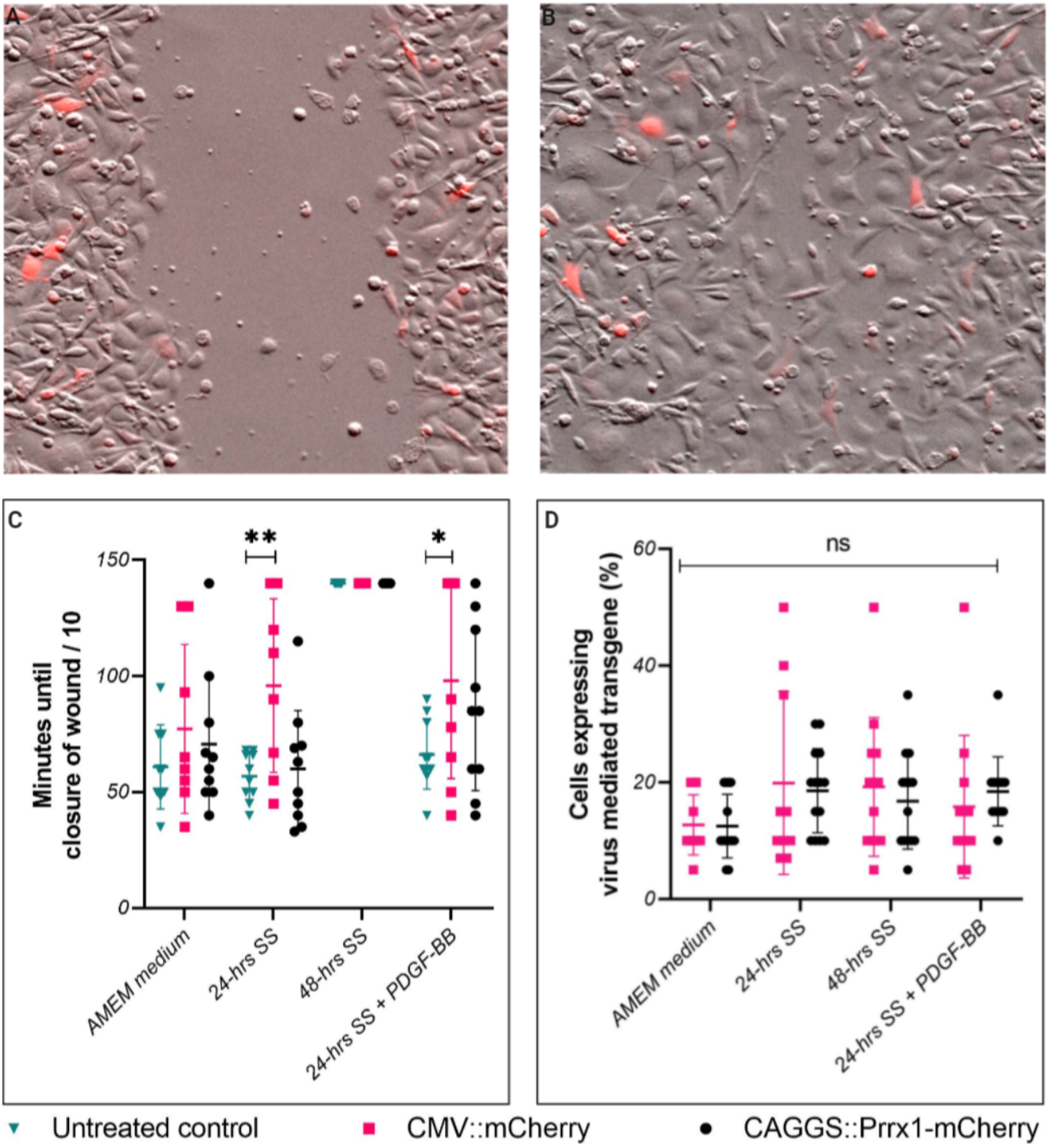

Figure 6: A and B: Illustrated is an AL1 cell culture, 10 and 690 minutes after scratching, respectively. B represents the point in time, when the scratch was considered closed, I.e. cells from both edges of the scratch have reached cells from the other side over the whole length of the wound. C: The time needed by cells to completely close a simulated scratch wound is shown. An untreated control group, a group infected with CMV::mCherry mock-virus, and a group infected with CAGGS::Prrx1-mCherry expressing baculovirus were used. (n=5) D: Percentage of AL1 cells that showed visible transgene expression upon infection with either the CMV::mCherry mock virus or CAGGS::Prrx1-mCherry baculovirus in different culture conditions. (n=7). (Two-stage linear step-up procedure of Benjamini, Krieger and Yekutieli, Q = 1%. Computations assume that all rows are sampled from populations with the same scatter (SD)). AMEM=minimum essential medium eagle alpha modification; SS= serum starvation; PDGF-BB=platelet-derived growth factor BB

We found that virus infection, but not *Prrx1* overexpression, had a significant influence on wound heal times. The mock-virus infected cells needed significantly longer to close the scratch than cells from the uninfected control, when subjected to a 24-hour growth period in serum-free medium or serum-free medium supplemented with PDGF-BB prior to introduction of the wound (Figure 6C). The proportion of infected AL1 cells was not significantly different between the two viruses (Figure 6D). As shown in Figure 6B, the lack of counterstaining made it impossible to reliably quantify the number of uninfected cells. The method of approximation is explained in the methods section below. We did not find a significant correlation between the proportion of infected cells in our samples and their respective wound heal times (not shown). In summary, the impact of viral infection on wound heal times raises to question the reliability of BV as an *in-vitro* gene transfection tool, a question we aimed to answer in subsequent experiments.

Effect of PTAL overexpression on cell proliferation

While *Prrx1* is an important gene in regeneration due to its role as a limb CT marker, microarray data brought forth another gene that showed interesting expression patterns during regeneration. PTAL was shown to be highly expressed during development and advanced stages of regeneration, but downregulated in the mature tissue in axolotl. Its curious expression profile makes PTAL a viable target for further experimental investigation. Its exact function is unclear, partly because it has no known orthologues in non-regenerating species. Prothymosin-

Alpha (ProTa), its nearest relative in non-regenerating animals, is a small, acidic, nuclear protein, widespread in many tissues and cell types. In the literature, accumulating evidence points towards a role of ProTa as a chromatin remodeling complex[38], involved in regulating cell proliferation by shortening G1 phase in different cell lines[39,40]. ProTa has also been shown to be secreted from neurons in a non-classical release mechanism[41]. While the same secretion was not experimentally verified for PTAL, computational models also predict such a mechanism for PTAL. Since neurons play an important role in the initiation and maintenance of regeneration in axolotl[42], this might be interesting for our research. Based on these findings, we argue that PTAL could act as a contributor to late-stage regeneration by stimulating proliferation, possibly in a neuron-dependent fashion. To determine the exact effect of differential expression of PTAL on axolotl limb CT cells, functional assays were carried out.

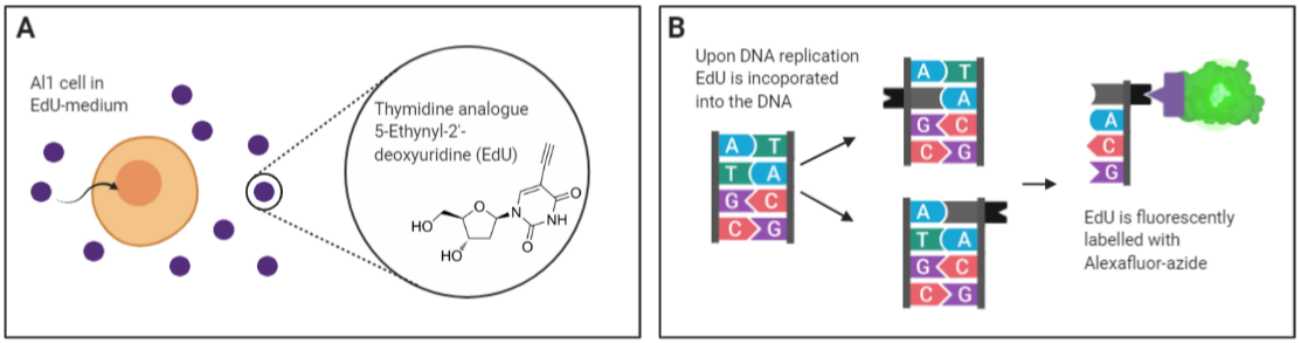

Figure 7: A: Depicted is an AL1 cell in EdU-enriched medium. The chemical structure of the thymidine analogue EdU is shown. B: The mechanism of EdU detection is illustrated. During DNA replication, EdU is incorporated into the DNA of the daughter cells in place of thymidine and can subsequently be detected by a click reaction with a fluorescently labeled azide. Shown here is the detection with alexafluor-488 (AF-488).

To determine the effect of PTAL overexpression on AL1 cell proliferation, we decided to carry out 5'-ethynyl-2'-deoxyuridine (EdU) staining, a simple and reliable method to determine cell proliferation rates[43].

EdU is a thymidine analogue, that is incorporated into the replicating DNA during S-phase[44] (Figure 7). Linking a fluorescently labeled azide to EdU in a click-reaction allows microscopic detection of cells that entered S-phase during EdU exposition (Figure 8). BV was once again used as a transfection method to confer PTAL overexpression in AL1 cells. Using this EdU-based approach, we were hoping to detect any changes in cell proliferation following BV mediated overexpression of PTAL in AL1 cells.

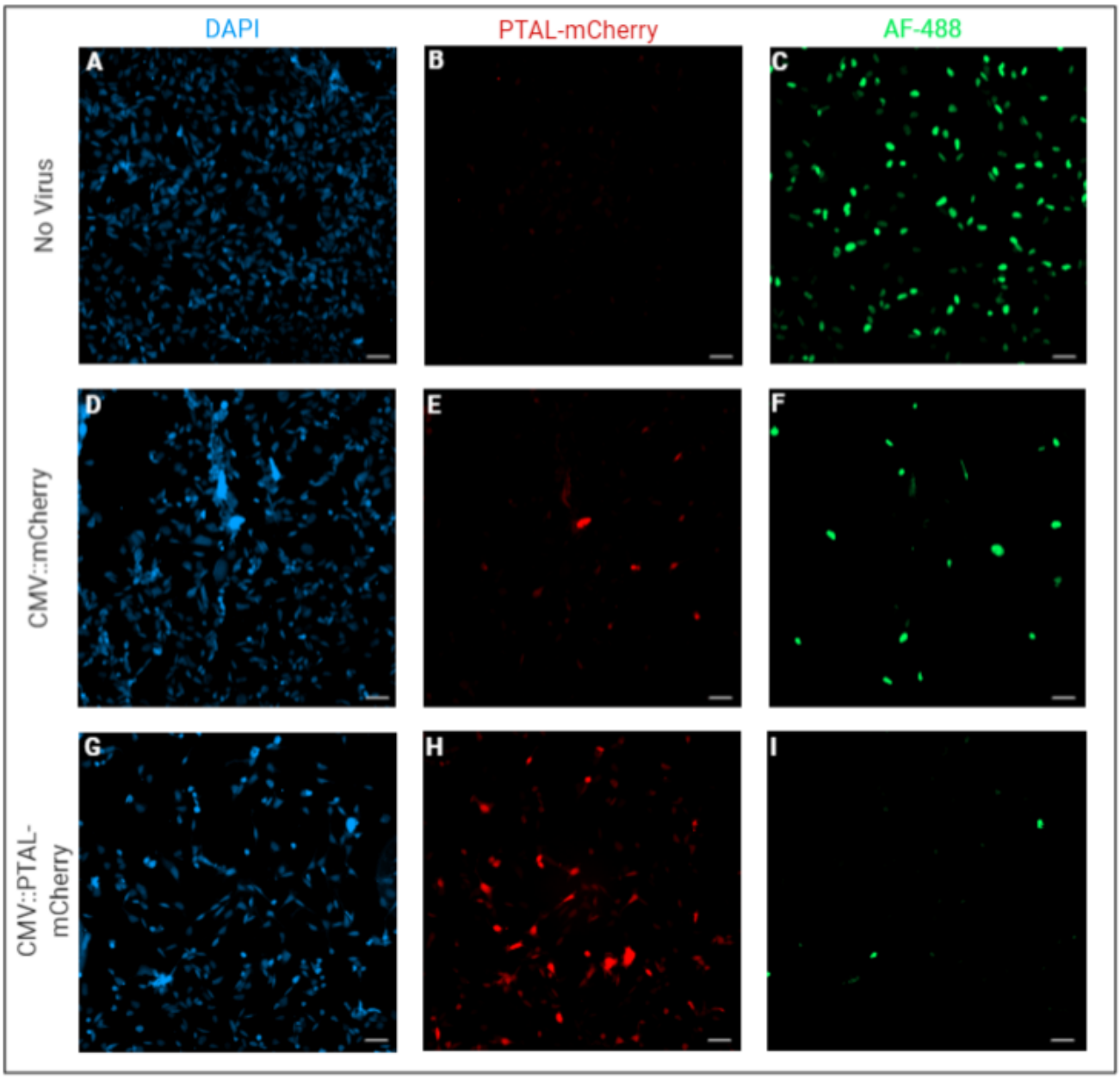

Figure 8: A-I: Microscopy images of EdU assays, carried out on AL1 cells infected with CAGGS::PTAL-mCherry and CMV::mCherry expressing baculovirus, respectively, as well as uninfected cells.

We found that viral infection seriously impaired cell proliferation, while PTAL overexpression had no discernible impact on cell division rate. Both the CMV::*mCherry* mock virus, and the CAGGS::PTAL-*mCherry* baculovirus negatively influenced the cell proliferation rate when compared to uninfected control groups. At the same time, the proportion of EdU^+ cells in the two infected groups were not different from each other (Figure 9A).

Both viruses were able to confer strong transgene expression in AL1 cells. The CAGGS::PTAL-*mCherry* expressing virus resulted in a visibly but not significantly, higher infection rate with stronger transgene expression (Figure 9B). These results clearly demonstrate the detrimental effect of viral infection on cellular fitness *in-vitro*, and we subsequently set out to better characterize the cytotoxic effect of BV on AL1 cells.

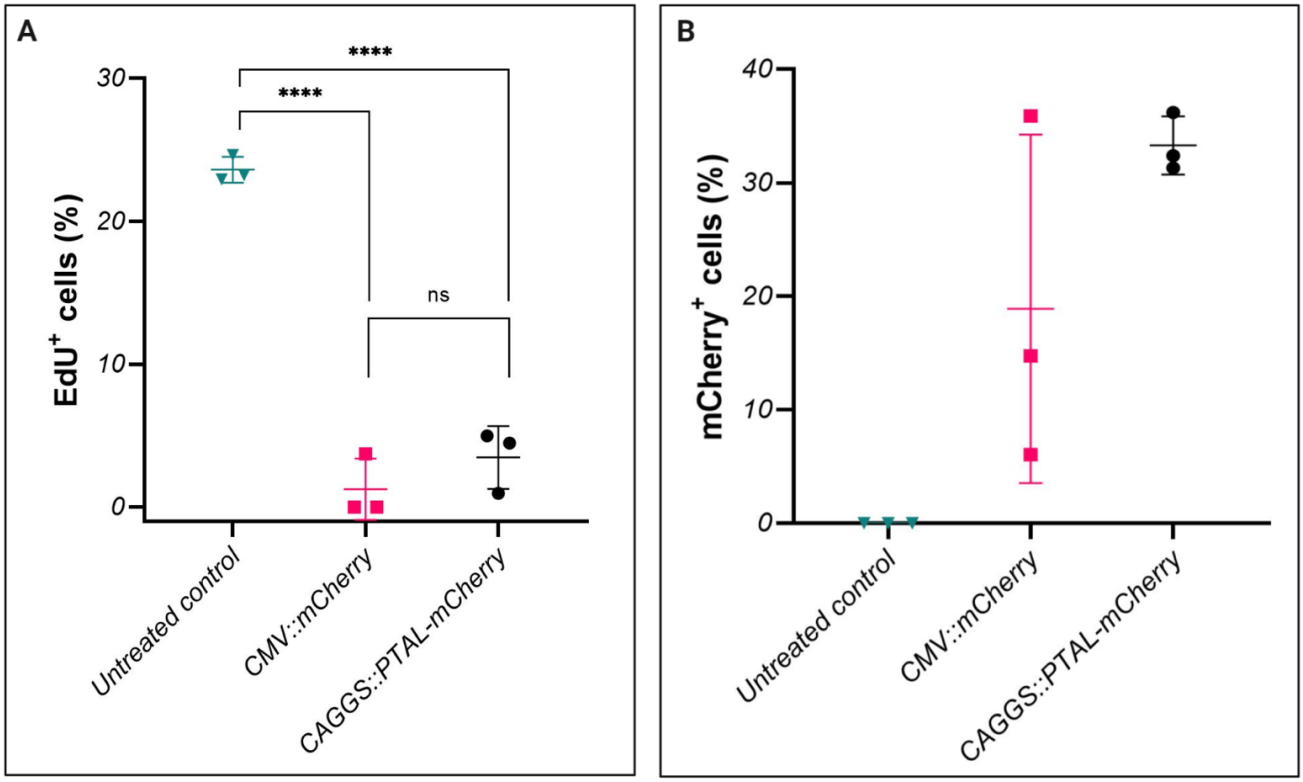

*Figure 9: A: Comparison of the proportion of EdU+ AL1 cells in culture infected with either CMV::mCherry or CAGGS::PTAL-mCherry expressing baculovirus. B: Proportion of mCherry+ AL1 cells in cultures infected with either CMV::mCherry or CAGGS::PTAL-mCherry expressing baculovirus. n=3, ordinary one-way ANOVA, ****=p<0.0001, ns=non-significant.*

Characterization of baculovirus-mediated cytotoxicity on AL1 cells *in-vitro*

The previous experiments strongly suggest that BV mediated cytotoxicity interferes with results from *in-vitro* assays. Therefore, we set out to investigate the adverse effects of BV infection on AL1 cells. On one

hand, a cell population needs to be properly infected to give conclusive results in an experiment. On the other hand, if a high infection rate causes a cell population enough stress to interfere with the results of the experiment, unchecked BV infection is not desirable either. An optimum between those two parameters might exist, where a cell population could be sufficiently infected to give conclusive experimental results, while BV mediated cytotoxicity is low enough to not interfere with experimental outcome. We therefore intended to titer the cytotoxicity of BV on AL1 cell cultures. For this purpose, we infected axolotl cells with increasing amounts of virus and performed EdU staining on them. We were hoping to determine a viral titer with which AL1 cells were successfully infected, while keeping the negative side effects to a bare minimum. The EdU assay was chosen, because cell proliferation rate was proven to be affected by BV infection.

Cytotoxicity of two viruses was assessed, both expressing only fluorophores under control of constitutive promoters. This way, we ruled out the possibility of functional transgenes interfering with our results. In a first step, the exact titer of the used BV was determined by dilution series titration on SF9ET cells. Virus 1 was a CMV::GFP encoding virus with an initial titer of $2x10^{7}$ pfu/mL, and virus 2 contained a CMV::mCherry construct and had an initial titer of $2x10^{10}$ pfu/mL. AL1 cells were then infected with different virus amounts. First, we wanted to determine whether the actual volume of viral prep used influenced cytotoxicity and infectivity. And secondly, we were interested in the effect of different final

viral titers on our cells. AL1 cells were infected with increasing volumes of either CMV::GFP or CMV::mCherry virus. The different initial virus titers of the two strains resulted in different final virus titers in our Al1 cultures (Table 2).

Table 4: Infection of AL1 cells with the same volumes of two BV samples with different initial titers. The viral load in plaque forming units (PFU) is correlated with the percentage of EdU+ cells and the percentage of cells that express the virally transmitted fluorophore (GFP+/mCherry+).

	CMV::GFP [b]			CMV::mCherry [c]		
Volume [a]	**PFU**	**EdU+ cells (%) ****	**GFP+ cells (%) *****	**PFU**	**EdU+ cells (%) ****	**mCherry (%) *****
0	0	18	0			
1	$2x10^2$	21	0	$2x10^5$	13	0
5	$1x10^3$	25	0	$1x10^6$	30	0
10	$5x10^3$	30	0	$5x10^6$	36	1
50	$1x10^4$	30	0	$2.5x10^7$	25	6
100	$5x10^4$	28	0	$1.25x10^8$	28	6
500	$2,5x10^5$	25	0	$6.25x10^8$	5	40

*Note. Correlation of viral titer with percentage of EdU^+ cells and percentage of fluorophore expressing cells, respectively, was calculated using the Pearson correlation coefficient with a two-tailed P-value. Confidence interval is 95%. [a] ul of 1/100 diluted initial virus stock. [b] Initial concentration of viral stock CAGGS::GFP: $2x10^7$. [c] Initial concentration of viral stock CMV::mCherry: $2x10^{10}$. ** $p < 0.01$ *** $p < 0.001$*

A 24-hour EdU pulse was used to mark proliferating cells, and after fixation, the cells were stained for EdU incorporation using AF-647. Analysis was done in Fiji, where first, cells were segmented based on DAPI staining, determining the absolute number of cells imaged. In a second step, the mean AF-647 intensity in those segments was measured. A cutoff value for this mean intensity was determined to differentiate EdU+ cells from EdU- cells. In a last step, the number of fluorophore-expressing cells was determined by manual counting, since automated detection of the cytoplasmic fluorophore signal was too unreliable.

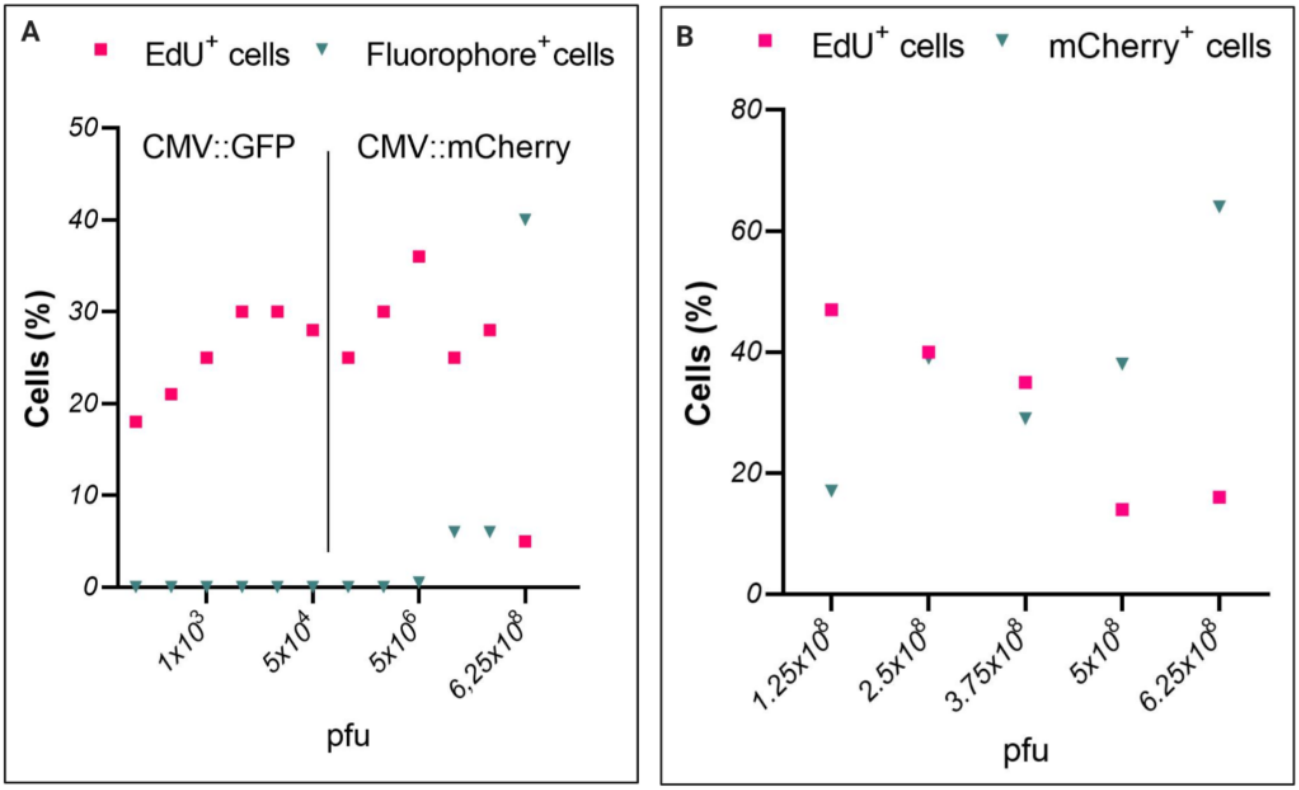

Figure 10: A: Plotted are the percentage of EdU+ and Fluorophore+ cells in Al1 cell cultures upon infection with BV. The first six samples were infected with CMV::GFP expressing BV with an initial titer of 2x10^7 pfu/mL. Shown on the right are samples infected with CMV::mCherry expressing baculovirus with an initial titer of 2x10^10 pfu/mL. B: Percentage of EdU+ and mCherry+ cells in AL1 cell cultures infected with CMV::mCherry expressing baculovirus.

Figure 10A depicts the percentage of EdU+ and fluorophore expressing cells in samples subjected to different viral loads. We noticed a sharp decline in EdU+ cells as well as a sudden increase of fluorophore expressing cells between 100ul and 500ul of 1/100 diluted CMV::*mCherry* encoding BV, corresponding with $2x10^7$ and $1x10^8$ BV-particles, respectively. Subsequently, we wanted to investigate this range in smaller intervals, to better resolve the progression of cytotoxicity and transgene expression. The results of this experiment are depicted in Figure 10B and demonstrate that cytotoxicity and transgene expression inversely correlate in a near-linear manner, with an optimum between these two

parameters around $5x10^8$ particles. These results suggest that BV has only limited viability as an *in-vitro* transfection method, and careful consideration of the respective virus is needed before conducting such *in-vitro* experiments.

Discussion

Blastema timecourse

We set out to analyze the spatial and temporal distribution of *Prrx1*$^+$ cells in both source zone and blastema over the course of two weeks following limb amputation. PRRX1 is a marker for limb CT cells in axolotl[31]. These cells play an important role during regeneration, since they have been shown to contribute greatly to blastema formation[21]. Which proportion of the blastema is formed by *Prrx1*$^+$ cells in different stages of regeneration has not been exactly determined until now. The combination of automated fluorescence microscopy and Cre-loxP based lineage tracing methods allowed us to characterize the spatiotemporal distribution of *Prrx1*$^+$ cells during limb regeneration in axolotl.

Prrx1$^+$ cells were determined by genomic mCherry and antibody-mediated AF-488 signal. We excluded skeletal cells from our quantification, since these were shown not to significantly support blastema formation and were easily excluded based on their location in the bone[21]. Also excluded were epidermal cells, seen in Figure 3 as a brightly green colored cell population on the edge of the sections. Epidermal cells were identifiable based on their orientation relative to

other tissue. A third cell population that was excluded from our counting were blood cells. Especially in the earlier sections, blood cells formed clusters that exhibited strong autofluorescence in the mCherry channel, which gave them a similar appearance to *Prrx1*$^{+}$ cells. They were identified by a distinct absence of fluorescence in their respective centers. *Prrx1*$^{-}$ cells were all cells that showed neither AF-488, nor mCherry signal. Using these parameters, we are confident that we were able to distinguish blastema forming CT cells from all others.

After devising the necessary classifications for cells, we went on to manually quantify *Prrx1*$^{+}$ cells instead of automating this task. A software-based, automated approach was considered, but the imaging data obtained did not allow this for several reasons. For once, the storage space needed for our images in a usable resolution would have been substantial. Secondly, the staining quality of sections from later timepoints, when the cell-density became increasingly higher, did not allow a proper segmentation of single cells and even less so for the distinction of *Prrx1*$^{+}$ and *Prrx1*$^{-}$ cells. A solution based on machine learning was considered, but rejected for three reasons: the time needed to implement such a solution would have been too high, meaning that even if the results were more reliable than manual analysis, it would have been not worth the additional time spent on the problem. Secondly, this approach would rely on a predefined training set, essentially a set of sections that was counted manually. Manual generation of these training data sets would ultimately defeat the purpose of implementing such a

tool. Lastly, we would have needed to manually inspect the quality of the results, further reducing the benefits of automation. Manual counting was considered the most efficient way to analyze *Prrx1*$^{+}$ cell distribution in our microscopy data.

The absolute numbers, as well as the respective proportion, of *Prrx1*$^{+}$ cells in both the source zone and the blastema were analyzed at different stages of limb regeneration. The steady increase in *Prrx1*$^{+}$ cells in the blastema over the course of regeneration (Figure 4A) was not surprising and can be explained by normal tissue growth. Interestingly, the proportion of *Prrx1*$^{+}$ cells in the blastema 5 dpa was significantly higher than in the source zone, while at the same time, the absolute number of cells at this stage did not differ significantly between the two regions. After amputation, the blastema is formed by CT cells that migrate from the source zone towards the amputation plane[21]. This means that *Prrx1*$^{-}$ cells are almost completely absent from the blastema at this stage. A small increase in *Prrx1*$^{+}$ cells, as seen in Figure 4A from 3 dpa to 5 dpa, therefore leads to a significant change in the ratio of *Prrx1*$^{+}$ to *Prrx1*$^{-}$ cells. Currie et al. showed in 2016 that this migration from the source zone to the blastema is a key contributor to limb regeneration but failed to report a proper quantification of this process[21]. Our data indicates that the proliferation of *Prrx1*$^{+}$ cells in the source zone, and their subsequent migration into the blastema, creates an equilibrium in the source zone from 7 dpa onward. From this point on, the source zone is stably comprised of 50-55% *Prrx1*$^{+}$ cells, representing about 450 cells per section.

The migration of *Prrx1*$^{+}$ cells from the source zone into the blastema, and their respective proliferation there, causes a vastly higher proportion of *Prrx1*$^{+}$ cells in the blastema.

The distribution of *Prrx1*$^{+}$ cells in source zone and blastema followed a uniform distribution until 10 dpa. During the early stages of regeneration *Prrx1*$^{+}$ cells are uniformly distributed, but at 14 dpa we could see a pattern of *Prrx1*$^{-}$ cells forming. In the proximal part of the blastema, an arrow shaped structure of *Prrx1*$^{-}$ cells formed as a prolongation of the bone from the source zone. At the same time, *Prrx1*$^{+}$ cells clustered with a high density at the distal part of the blastema (Figure 3E). This pattern was visible in every section from this timepoint, making a random pattern, caused by variances in antibody staining, unlikely. CT cells have been shown to reconstitute different parts of the limb by successive migration of distinct cell populations into the blastema[21]. Periskeletal cells are among the first cell types to migrate to the blastema to extend the severed bone at the amputation plane. Dermal fibroblasts subsequently regenerate the distal limb proportions at a later stage. Our observed *Prrx1*$^{+}$ cell distribution could signify the transition between these two stages. The loss of *Prrx1* expression in the proximal blastema could represent the differentiation of multipotent progenitor cells into mature cells of the regenerated limb.

Production protocol optimization

The BV production protocol was optimized to allow Cas9-BV production. Cas9-containing DNA constructs often exceed the maximum

length conventional tools can transfect into target cells. BV was adopted as a gene transport vehicle specifically because no maximum insert length is known for it, which would allow for efficient knock-out of genes *in-situ*. The increased length of Cas9 containing recombinant cassettes made the production of Cas9-BV challenging, and caveats in the production protocol were identified and eliminated. Molecular integrity and purity of the bacmid were shown to be crucial for successful Cas9-BV formation. We also propose the formation of defective interfering virus particles (DIVP) as a possible explanation for several unexpected observations during Cas9-BV production.

The stoichiometry between bacmid and shuttle vector, the molecular integrity and the purity of the bacmid were suspected to influence the efficiency of BV formation. For BV production, the bacmid, containing a replication incompetent viral genome, and a shuttle vector with a recombinant cassette and a repair template for the defective genes are transfected into SF9 insect cells. The SF9 cells reconstitute a functional viral genome via homology directed repair, while simultaneously introducing the recombinant cassette into the viral genome. Introducing a double-strand break by digesting the bacmid with the SbfI restriction enzyme greatly increases the efficiency of this repair process. Because of the immense length of the bacmid, the resulting loose ends are exposed to strong shear forces, degrading the DNA sequence over time. We noticed a decline in virus formation over time with increasing age of digested bacmid prep. By preparing the bacmid digest freshly, we were

able to solve this problem, and increase the efficiency. Next, we wanted to determine the effect of different ratios between bacmid and shuttle vector on recombination efficiency. The immense length of the bacmid shifts the stoichiometry of bacmid and shuttle vector in the recombination reaction towards an excess of shuttle vector. We wanted to counter this by increasing the amount of bacmid in contrast to shuttle vector. Surprisingly, no effect of stoichiometry on the recombination efficiency was discernible. We decided to pursue a different approach to optimize recombination efficiency. From written correspondence with other facilities we learned that bacmid preps contain up to 60% contamination with genomic DNA from E. coli. We were arguing that a more effective purification process could translate into an increase in recombination efficiency by reducing the amount of contamination DNA. Following my departure from the project, Helena Okulski was able to produce Cas9-BV by using bacmid that was purified with a kit, optimized for extremely long DNA constructs. Even with these optimizations, the production of BV from shuttle vectors exceeding 10kb in length was hardly possible. In the future, the recombination efficiency of bacmid and shuttle vector could be further increased by introducing an additional cut on the shuttle vector. More double strand breaks for the DNA repair machinery to recognize could have a positive impact on the efficiency of virus production. Even as optimizations to the protocol allowed for Cas9-BV production, the reason for the initial failures is not completely clear.

During our unsuccessful Cas9-BV production attempts, we made several unexpected observations (Table 3). Starting with bacmid and shuttle vector transfection into SF9 cells, we were able to observe signs for both successful virus formation, and signs that no functional BV was formed. The typical bloating of SF9 cells following viral infection was clearly visible during the whole virus amplification process. At the same time, these bloated SF9 cells did not show expression of fluorophores that ought to be present on the respective recombinant cassettes. We knew from earlier work that SF9 cells typically express fluorophores upon transfection, as long as they are not co-transfected with Cas9. Fluorophore expression was also absent in subsequent infections of AL1 cells with Cas9-BV, again indicating the absence of functional BV. At the same time, when carrying out a dilution series titration on SF9ET cells, expression of GFP in those cells clearly shows presence of BV. These odd observations could be caused by formation of defective interfering virus particles (DIVP).

DIVP are commonly observed during virus production and could explain the behavior of SF9 cells during Cas9-BV production. First identified in RNA viruses, DIVP are viruses that are missing an essential part of their genome. They are usually able to infect host cells on their own, but are unable to replicate after infection. Since their discovery, DIVP have been observed in a wide range of RNA and DNA virus species, making their presence in BV plausible. DIVP arise, when a part of the viral genome is lost during reproduction, for example via template switching.

The defective genomes are then packaged into virus particles and can infect other cells. Once introduced into other host cells, they are not able to properly replicate, because of the absence of essential proteins like for example viral polymerases. When a cell is co-infected by both DIVP and functional virus, the essential proteins are supplied by the functional virus, and shared between DIVP and functional virus. Typically, the shorter genome length of DIVP leads to decreased replication times, which mean that DIVP can outcompete functional virus over time. DIVP formation could explain the observations made during Cas9-BV production. Considering that DIVP are typically able to infect host cells, the characteristic bloating of SF9 cells upon transfection with bacmid and shuttle vector can be explained by presence of DIVP in the cell. The concurrent absence of fluorophore can be explained by a loss of the fluorophore gene during DIVP formation. A minimal amount of functional virus would be sufficient to enable the amplification of massive quantities of DIVP, explaining the enduring absence of fluorophore with simultaneous bloating of SF9 cells during the whole length of virus propagation. GFP expression in SF9ET cells during titration can also be explained by presence of DIVP. SF9ET cells contain a GFP encoding gene under control of the viral polyhedrin promoter. In the presence of virus, the polyhedrin promoter is active and GFP is expressed, allowing the reliable detection of BV in SF9ET cultures. Upon infection with DIVP, the GFP gene would be activated, if the necessary transcription factors are still present on the viral genome, without allowing distinction between

functional and defective virus. Considering the reproduction mechanism of DIVP, amplification of virus in new SF9 cultures should in the future be initiated with as little virus as possible to reduce the probability of infection with DIVP.

Scratch assay

After demonstrating the widespread expression of *Prrx1* throughout limb regeneration, we wanted to determine its function. We conducted scratch assays to determine the effect of *Prrx1* overexpression on the ability of AL1 cells to close a simulated scratch wound *in-vitro*, and chose BV as our method of transfection. BV has only seen limited testing *in-vitro*, therefore these experiments also aimed to characterize the effect of virus infection on AL1 cells. To gain a better understanding of AL1 cell behavior, we conducted overexpression experiments in different culture conditions. The results of this wound heal experiment furthered our understanding of cellular behavior under a variety of different conditions.

To analyze the behavior of AL1 cells during wound healing, we measured the time needed to close the scratch, and the proportion of *mCherry*$^{+}$ cells in the test groups. The scratch was considered closed, when cells from both sides met each other over the whole length of the scratch, but the slow and erratic movement of AL1 cells caused a certain ambiguity of the exact point of closure. Going forward, an automated solution for this problem could be used if fluorophore expressing cells were available. Fluorophore expressing AL1 cells would allow the proper segmentation and calculation of cell-free space in the scratch area and

enable exact determination of wound closing behavior. The employment of fluorophore expressing cells would also allow to exactly determine the percentage of $mCherry^+$ cells in cultures by providing a counterstaining of uninfected cells. Due to a shortage of GFP^+ AL1 cells, we could not implement these additional measures in our approach. Nevertheless, we were able to sufficiently measure wound heal time and BV infection, and in the future, the use of fluorophore expressing AL1 cells can further increase the accuracy of this data.

Supplementation of PDGF-BB did not significantly decrease wound heal times, but serum starvation 24 hour before and after wounding greatly affected the time necessary to close the scratch. Cells subjected to a 48-hour long serum starvation pulse were not able to close the scratch over the course of 24 hours. This is in line with previous work that indicated a detrimental effect of serum starvation on various functions of cells *in-vitro*[37]. Interestingly, we did not see an effect of PDGF-BB supplementation on wound heal time, as reported by Currie et al[21]. Our own approach differed from their experimental setup in several ways: Currie et al. were conducting their experiments with primary GFP^+ blastema cells, whereas we wanted to investigate the behavior of AL1 cells during wound healing. They cultivated their cells in serum free medium from the beginning and supplemented this medium after wounding with 1% fetal calf serum or PDGF-BB, respectively. In our approach, on the other hand, we initially cultivated our cells in 10% serum supplemented AMEM, because we were observing increased cell death in

prolonged absence of serum. We then subjected our samples from the respective groups to a 24-hour serum starvation pulse prior to wounding and allowed the cells to heal the wound in presence of serum. The switch from starvation during healing to starvation prior to healing could explain why PDGF-BB supplementation during the starvation pulse had no effect on heal times. Our cell line could be more sensitive to the absence of serum than primary blastema cells, explaining why we had trouble maintaining an initial culture in serum free medium. Residual serum, from the initial culture conditions, on cells during the starvation pulse could also play a role in the different observations. And lastly, their primary cell line could be more susceptible to PGDF-BB supplementation than AL1 cells. In the future, a fluorophore expressing AL1 cell line could be used to exactly replicate the experimental conditions of Currie et al. Our results demonstrate that culture conditions greatly impact cell behavior *in-vitro* and must be carefully considered before conducting any experiments with AL1 cells.

Our data suggests that virus infection, but not overexpression of *Prrx1*, significantly affected wound heal times *in-vitro*. *Prrx1* overexpression did not lead to changes of the wound close times when compared to mock-virus infected control groups. This was consistent across all culture conditions. Remarkably, samples infected with CMV::mCherry expressing mock-virus needed significantly longer to close scratch wounds than uninfected control samples in two culture conditions. Considering that mCherry expression does not mechanistically impair cell motility, this

result implies that virus infection somehow reduces the ability of AL1 cells to migrate into the introduced wound. We therefore compared the percentage of cells that showed virus mediated transgene expression but could not see a significant difference between mock and *Prrx1* expressing virus (analysis not shown). We also found that the percentage of infected cells in a sample did not significantly correlate with its respective wound heal time (analysis not shown). These results imply a cytotoxic effect of BV infection on AL1 cells *in-vitro*, but the generated data is insufficient to properly characterize this cytotoxicity. It seems that *Prrx1* overexpression does not influence wound healing times, but we do not rule out the possibility that such an effect could be masked by BV mediated cytotoxicity in this assay. To further characterize the role of *Prrx1* in cell motility in the future, knock-out experiments are needed to also investigate the behavior of AL1 cells in the absence of *Prrx1*.

PTAL EdU assay

We decided to investigate the effect of PTAL overexpression on cell proliferation, but BV mediated cytotoxicity obfuscated any potential effects of PTAL overexpression. A role of PTAL in cell proliferation was plausible from literature research and expression profiles from earlier work[22,39,40]. We used the EdU assay, a straightforward experiment to label cells that enter S-Phase, to investigate cell proliferation rates in AL1 cells. Both our CMV::*mCherry* mock virus treated group, as well as the group infected with CAGGS::PTAL-*mCherry* expressing BV showed a significant decrease in EdU+ cells. Indicating that BV infection, and not BV mediated

overexpression of PTAL, caused the change in cell proliferation. Combined with results from scratch assays, these data proves the cytotoxic effect of BV infection on AL1 cells, which needs to be further investigated.

Baculovirus titration on AL1 cells

After we observed a significant reduction of AL1 cell proliferation following BV infection, we decided to determine the effect of different virus amounts on AL1 cells in EdU assays. The virus could affect AL1 cells via direct interaction, meaning that the infection process and subsequent hijacking of cellular processes by the virus inhibits cell proliferation of AL1 cell. Another possibility would be contamination of cell culture with residues from the virus production process. Cellular debris from insect cells, SF9 cell-derived proteins, and buffer and sucrose residues could interfere with AL1 cell behavior. In the former case, the final virus titer in cell culture should consistently affect the cell proliferation rate, while in the latter scenario, the volume of virus used in an assay should influence cellular behavior. We therefore infected AL1 cells with the same volumes of two viruses with different titers. This allowed us to investigate both the effect of different virus volumes and the effect of different virus titers on AL1 cells. As shown in experiments investigating the effect of PTAL overexpression on AL1 cells, the EdU assay proves sensitive to viral infection (Figure 9A). We could determine the influence of BV titer, but not volume, on the proliferation of the host cells. Infection rate also increased

with final virus titer in culture, and an optimum between these two parameters does exist.

We were able to determine a viral load in the AL1 culture, where the targeted cells showed infection, while the decrease in proliferation is still minimal. The consistency of this point in different experimental setups is questionable, and dependent on several factors. BV with a higher initial titer may be able to infect cells more efficiently, meaning that two viruses with different initial titers could result in a different penetrance of infection, even if used in the same final titers. The experimental setup from above could be slightly modified to answer this question, by increasing the volumes of the lesser concentrated virus. Age of the virus is another factor contributing to the infectivity of BV. If stored properly, BV can reliably infect axolotl cells for up to six months, but we noticed a continuous decline in infectivity over this period. It would be interesting to see if a decline in infectivity over time also coincides with a decrease in cytotoxicity, which would indicate that the virus's ability to infect the host cell, but not the number of viral particles, affects cytotoxicity. In this experiment we were only investigating the cytotoxic effect of BV on AL1 cells, while cells from other organisms could react differently. Not only the type, but also the condition of the host cells influences their ability to mitigate virus-induced cytotoxicity. Age and confluency are examples for features of a cell culture that may influence their ability to deal with virus infection, or at least influence the result of the assay used.

Taken together, BV should be used with caution in *in-vitro* settings, and if possible, replaced by less invasive methods. A titration experiment as outlined in this thesis is needed whenever BV is used *in-vitro*, to characterize the reaction of the target cell culture to viral infection. Nonetheless, BV remains an important tool for *in-vivo* transduction, since cytotoxicity in live animals is negligible.

Methods

Blastema connective tissue cell counting

Cells were counted in the regenerated part of the limb as well as the cells in the source zone, located in the 500µm preceding the amputation plane. Counting was done in Fiji[45]. Before the counting, the images were exported from the application "CaseViewer" (3dHistech) which is designed to view images produced by a slide scanner. The best sections were identified, and the image was opened in the cell counter plug-in from Fiji. The amputation plane was marked with a straight line to separate blastema from source zone. The proximal end of the source zone was marked to designate the area to count in. Skeletal cells were counted based on bone morphology, extra care needs to be taken not to mark periskeletal cells. The red and green channels were used to identify *Prrx1*$^{+}$ cells. Then *Prrx1*$^{-}$ cells were identified by switching to the blue channel and counting all the cells that have not been marked yet.

Bacmid digestion

Bacmid was amplified in DH10 E. coli strain (Macherey-Nagel NucleoBond XtraMaxi, Catalog number: 740414.10) and isolated by maxiprep (Thermo Scientific GeneJET Plasmid Maxiprep Kit, Catalog number: K0491). The last step of the prep was done under sterile conditions. Bacmid was digested with SbfI RE (New England Biolabs, Catalogue number: R3642S) for 4 hours at 36°C, and enzyme was inactivated at 80°C for 20 minutes.

SF9 culture

SF9 cells (Expression Systems # 94-001F) were obtained from VBCF Protec facility in Vienna and cultured in ESF921 serum-free medium (Expression Systems, catalogue number: 96-001-01) at 27°C in 2% CO2 at 200 rpm.

SF9 transfection

0.8 mL ESF921 medium without any antibiotics were filled in 24-Well Blocks (Qiagen, catalogue number: 19583), that were rinsed with 70% ethanol beforehand to get rid of chemical residues from the production process. DefBac bacmid was added to the medium. The amount was dependent on the quality of the bacmid prep (approximately 5ul). An appropriate amount of shuttle vector was added (200ng or 1ul, again, the final amount needed for transformation to work may vary), along with 12ul Escort IV (Sigma-Aldrich, catalogue number: L3287) and incubated at room temperature for 20 minutes. Afterwards the SF9 cells were added in

a concentration of $5x10^6$ cells/mL to a final concentration of 10^6 cells/mL. BreathEasy (SIGMA #Z380059-1PAK) tape was used to seal the plate, and the mixture was put to shake with 200 rpm at 27°C. After three hours, another mL of medium was added, and the cells were left to incubate for 4 days. After four days, successful infection was verified by examinatin of cell-bloat and fluorophore expression. After centrifugation (300xg, 5 min, 4°C), the supernatant (=P1 virus prep) was filtered and used to infect a new SF9 culture at $5x10^5$ cells/mL with as little P1 as possible (10ul-500ul) to keep DIVP formation as low as possible. The freshly infected SF9 culture was then incubated for 5 more days, and the supernatant following centrifugation (300g, 10 min, 4°C) was sterile filtered and stored for long term use at 4°C in the dark. P3 was produced as needed by infecting a 500 mL SF9 culture at a density of $5x10^5$ with 1 mL P2.

AL1 infection with baculovirus

Infection was carried out in a suspension culture, as dark as possible to not damage the virus with light. 1mL AMEM was put into a 24 well plate well along with 1-5µl concentrated BV. The exact amount of virus needs to be determined experimentally. 10^5 AL1 cells were added to the virus containing medium in the well and incubated at 27°C. After 48hrs fluorescent protein expression should be detectable under the microscope.

Baculovirus titration on SF9ET cells

In a 96 well plate (Greiner, catalogue number M3186) 100ul ESF921 medium per well was filled. BV was diluted 1/10000 and 25ul diluted BV were added to the well of the first row. The solution was mixed 5x with the pipette, and 25ul were transferred to the next row to create a 1:5 dilution series. 100u of SF9ET cells with a density of 250000 cells/mL were added to each well, starting with the most diluted rows. The plate was incubated for 6 days in the dark without shaking. Analysis was done by observation of wells that showed GFP expression and subsequent analysis in excel. The excel analysis sheet was obtained from Christian Aigner from the VBCF ProTec facility in Vienna.

Scratch assay

In a glass-bottomed 24 well plate (Eppendorf, catalogue number: EP0030741021) 100000 Al1 cells were seeded in 1mL AMEM medium (Stemcell Technologies, catalogue number: #36450) and let incubate for 48 hours. Afterwards, the medium was changed to the necessary culture conditions (AMEM, serum-free AMEM, serum-free AMEM + 15ng/mL PDGF-BB) and let continue to incubate for 24 hours. After 24 hours, a scratch was introduced with white pipetting tips (10ul1). The wells were rinsed with serum-free medium, and then filled up with their respective culture mediums again, before subsequently being imaged every 10 minutes for 24 hours in the cell discoverer microscope (Zeiss) with a 5x objective.

EdU assay

EdU staining for detection of cell proliferation was done using the Click-It EdU kit from Thermofisher (catalogue number: C10337) according to protocol.

References

I have made a reasonable effort to identify image owner(s) and in order to attempt obtain their consent for the use of images in this work. Should a copyright infringement nevertheless become known , I request that you notify me.

1. Marshall, C. D. *et al.* Cutaneous Scarring: Basic Science, Current Treatments, and Future Directions. *Adv. Wound Care* **7**, 29–45 (2018).
2. Tanaka, E. M. The Molecular and Cellular Choreography of Appendage Regeneration. *Cell* **165**, 1598–1608 (2016).
3. Gonzalez, A. C. de O., Costa, T. F., Andrade, Z. de A. & Medrado, A. R. A. P. Wound healing - A literature review. *An. Bras. Dermatol.* **91**, 614–620 (2016).
4. Driskell, R. R. *et al.* Distinct fibroblast lineages determine dermal architecture in skin development and repair. *Nature* **504**, 277–281 (2013).
5. Correa-Gallegos, D. *et al.* Patch repair of deep wounds by mobilized fascia. *Nature* **24**, 23–31 (2019).
6. Reinke, J. M. & Sorg, H. Wound Repair and Regeneration. *Eur. Surg. Res.* **49**, 35–43 (2012).
7. Rosenbloom, J., Macarak, E., Piera-Velazquez, S. & Jimenez, S. A. Human Fibrotic Diseases: Current Challenges in Fibrosis Research. in 1–23 (2017). doi:10.1007/978-1-4939-7113-8_1.
8. Tanaka, E. M. & Reddien, P. W. The Cellular Basis for Animal Regeneration. *Developmental Cell* vol. 21 172–185 (2011).
9. McCusker, C. & Gardiner, D. M. The Axolotl Model for Regeneration and Aging Research: A Mini-Review. *Gerontology* **57**, 565–571 (2011).
10. Wagner, D. E., Wang, I. E. & Reddien, P. W. Clonogenic neoblasts are pluripotent adult stem cells that underlie planarian regeneration. *Science (80-.).* **332**, 811–816 (2011).
11. Rink, J. C. Stem cell systems and regeneration in planaria. *Development Genes and Evolution* vol. 223 67–84 (2013).
12. Campbell, R. D. Tissue dynamics of steady state growth inHydra littoralis. II. Patterns of tissue movement. *J. Morphol.* **121**, 19–28 (1967).
13. Bode, H. R. The interstitial cell lineage of hydra: A stem cell system that arose early in evolution. *Journal of Cell Science* vol. 109 1155–1164 (1996).
14. Agata, K., Saito, Y. & Nakajima, E. Unifying principles of regeneration I: Epimorphosis versus morphallaxis. *Dev. Growth Differ.* **49**, 73–78 (2007).
15. Technau, U. *et al.* Parameters of self-organization in Hydra aggregates. *Proc. Natl. Acad. Sci. U. S. A.* **97**, 12127–12131 (2000).

16. Zakrzewski, W., Dobrzyński, M., Szymonowicz, M. & Rybak, Z. Stem cells: Past, present, and future. *Stem Cell Research and Therapy* vol. 10 68 (2019).
17. Wilgus, T. A. Regenerative healing in fetal skin: a review of the literature. *Ostomy. Wound. Manage.* **53**, 16–31; quiz 32–3 (2007).
18. Tam, J. *et al.* Reconstitution of full-thickness skin by microcolumn grafting. *J. Tissue Eng. Regen. Med.* **11**, 2796–2805 (2017).
19. Gerber, T. *et al.* Single-cell analysis uncovers convergence of cell identities during axolotl limb regeneration. *Science (80-.).* **362**, eaaq0681 (2018).
20. Campbell, L. J. & Crews, C. M. Molecular and cellular basis of regeneration and tissue repair: Wound epidermis formation and function in urodele amphibian limb regeneration. *Cellular and Molecular Life Sciences* vol. 65 73–79 (2008).
21. Currie, J. D. *et al.* Live Imaging of Axolotl Digit Regeneration Reveals Spatiotemporal Choreography of Diverse Connective Tissue Progenitor Pools. *Dev. Cell* **39**, 411–423 (2016).
22. Knapp, D. *et al.* Comparative Transcriptional Profiling of the Axolotl Limb Identifies a Tripartite Regeneration-Specific Gene Program. *PLoS One* **8**, e61352 (2013).
23. Kragl, M. *et al.* Cells keep a memory of their tissue origin during axolotl limb regeneration. *Nature* vol. 460 60–65 (2009).
24. Nowoshilow, S. *et al.* The axolotl genome and the evolution of key tissue formation regulators. *Nature* **554**, 50–55 (2018).
25. Khattak, S. *et al.* Optimized axolotl (Ambystoma mexicanum) husbandry, breeding, metamorphosis, transgenesis and tamoxifen-mediated recombination. *Nat. Protoc.* **9**, 529–540 (2014).
26. Fei, J. F. *et al.* Efficient gene knockin in axolotl and its use to test the role of satellite cells in limb regeneration. *Proc. Natl. Acad. Sci. U. S. A.* **114**, 12501–12506 (2017).
27. Oliveira, C. R. *et al.* Pseudotyped baculovirus is an effective gene expression tool for studying molecular function during axolotl limb regeneration. *Dev. Biol.* **433**, 262–275 (2018).
28. Hornstein, B. D., Roman, D., Arévalo-Soliz, L. M., Engevik, M. A. & Zechiedrich, L. Effects of circular DNA length on transfection efficiency by electroporation into HeLa cells. *PLoS One* **11**, (2016).
29. A. Lea, R. & K. Niakan, K. Human germline genome editing. *Nature Cell Biology* vol. 21 1479–1489 (2019).
30. Nohno, T. *et al.* A chicken homeobox gene related to drosophila paired is predominantly expressed in the developing limb. *Dev. Biol.* **158**, 254–264 (1993).
31. Logan, M. *et al.* Expression of Cre recombinase in the developing mouse limb bud driven by aPrxl enhancer. *genesis* **33**, 77–80 (2002).
32. Vincent, C. D., Rost, F., Masselink, W., Brusch, L. & Tanaka, E. M. Cellular dynamics underlying regeneration of appropriate segment number during axolotl tail regeneration Regeneration and repair. *BMC Dev. Biol.* **15**, 48 (2015).
33. Brabletz, T., Kalluri, R., Nieto, M. A. & Weinberg, R. A. EMT in cancer. *Nat. Rev. Cancer* **18**, 128–134 (2018).
34. Williams, E. D., Gao, D., Redfern, A. & Thompson, E. W. Controversies around epithelial–mesenchymal plasticity in cancer metastasis. *Nat. Rev. Cancer* (2019) doi:10.1038/s41568-019-0213-x.
35. Ocaña, O. H. *et al.* Metastatic Colonization Requires the Repression of the Epithelial-

Mesenchymal Transition Inducer Prrx1. *Cancer Cell* **22**, 709–724 (2012).
36. Dhillon, P. K., Li, X., Sanes, J. T., Akintola, O. S. & Sun, B. Method comparison for analyzing wound healing rates. *Biochem. Cell Biol.* **95**, 450–454 (2017).
37. Rashid, M. ur & Coombs, K. M. Serum-reduced media impacts on cell viability and protein expression in human lung epithelial cells. *J. Cell. Physiol.* **234**, 7718–7724 (2019).
38. Gómez-Márquez, J. & Rodríguez, P. Prothymosin α is a chromatin-remodelling protein in mammalian cells. *Biochem. J.* **333**, 1–3 (1998).
39. Wu, C. L., Shiau, A. L. & Lin, C. S. Prothymosin alpha promotes cell proliferation in NIH3T3 cells. *Life Sci.* **61**, 2091–101 (1997).
40. Smith, M. *et al.* Prothymosin alpha gene expression correlates with proliferation, not differentiation, of HL-60 cells. *Blood* **82**, 1127–1132 (1993).
41. Halder, S. K., Matsunaga, H. & Ueda, H. Neuron-specific non-classical release of prothymosin alpha: A novel neuroprotective damage-associated molecular patterns. *J. Neurochem.* **123**, 262–275 (2012).
42. Satoh, A., Gardiner, D. M., Bryant, S. V. & Endo, T. Nerve-induced ectopic limb blastemas in the axolotl are equivalent to amputation-induced blastemas. *Dev. Biol.* **312**, 231–244 (2007).
43. Chehrehasa, F., Meedeniya, A. C. B., Dwyer, P., Abrahamsen, G. & Mackay-Sim, A. EdU, a new thymidine analogue for labelling proliferating cells in the nervous system. *J. Neurosci. Methods* **177**, 122–130 (2009).
44. Zhao, H. *et al.* DNA damage signaling, impairment of cell cycle progression, and apoptosis triggered by 5-ethynyl-2′-deoxyuridine incorporated into DNA. *Cytom. Part A* **83**, 979–988 (2013).
45. Schindelin, J. *et al.* Fiji: An open-source platform for biological-image analysis. *Nature Methods* vol. 9 676–682 (2012).